
CHEMISTRY
OF THE ATMOSPHERE

Plasma and Electromagnetic Effects in the Ionosphere Related to the Dynamics of Charged Aerosols in the Lower Atmosphere

V. M. Sorokin

Pushkov Institute of Terrestrial Magnetism, Ionosphere, and the Radio Wave Propagation, Russian Academy of Sciences, Troitsk, Moscow oblast, 142092 Russia

Received June 8, 2006

Abstract—The paper presents a physical model of the electrodynamic effect on the ionosphere of natural and artificial processes that occur in the near-Earth atmospheric layer and are accompanied by the transfer of charged aerosols in the atmosphere. These processes include the preparation of earthquakes and typhoons, dust storms, and nuclear accidents. The model is based experimentally on satellite and ground-based records of plasma and electromagnetic perturbations, measurements of the injection of soil gases into the atmosphere, and atmospheric radioactivity data. The ionosphere is subject to actions of the conduction electric current flowing in the atmosphere–ionosphere circuit. Its source is an extraneous current formed by vertical turbulent transfer of charged aerosols and their interaction with atmospheric ions during the injection of radioactive substances and modification of atmospheric conductivity. Changes in the electric field of the ionosphere induce the development of plasma and electromagnetic phenomena. The model suggested relates ionospheric and electromagnetic perturbations to the dynamics of charged aerosols in the lower atmosphere.

DOI: 10.1134/S199079310702008X

1. INTRODUCTION

Numerous observations of anomalous plasma and electromagnetic phenomena in the ionosphere above the regions of seismic and meteorological activity [1–15] are evidence that intense processes in these regions influence the state of the circumterrestrial plasma during periods of from several hours to several dozens of days. The results of experimental studies performed on satellites show that processes in the Earth's lithosphere are related to electromagnetic and plasma perturbations in the ionosphere. These results were discussed in several reviews [16–21]. It can be suggested that ionospheric effects arise as a result of the simultaneous actions of various factors, such as acoustic waves, electric fields, electromagnetic radiation, chemically active substances, etc. An important role in the formation of these factors is played by aerosols of the lower atmosphere, which influence its conductivity and generate extraneous electric currents. Seismic activity is accompanied by the injection of soil aerosols into the atmosphere. Meteorological processes are related to the dynamics of aerosols existing in the atmosphere.

An analysis of satellite data showed the presence of electromagnetic perturbations over a broad spectral interval. These perturbations are localized within a magnetic field tube conjugated with the seismic focus of an impending earthquake. Data on electromagnetic radiation spikes in extremely and very low-frequency ranges in the ionosphere were obtained in [4–6, 11, 22]. Electromagnetic radiation spikes at ultralow frequen-

cies in the ionosphere were recorded in [3, 23]. In addition, electromagnetic radiation in this frequency range was recorded on satellites and in seismically active regions simultaneously [24], which showed that these phenomena were related to an increase in seismic activity. The reliability of the results obtained by recording electromagnetic radiation in the ionosphere was substantiated by statistical analyses of large arrays of satellite data on tens and hundreds of earthquakes [13, 25]. The amplitude of geomagnetic pulsations of magnetospheric sources in the ultralow-frequency range recorded on the Earth's surface was found to decrease several days before an earthquake [26]. Perturbations of the DC electric field in the ionosphere and the lower atmosphere related to seismic activity [3, 16, 27–31] and electron density fluctuations of up to 10% with 1 Hz periods in the ionosphere above the region of earthquake preparation [14] were also observed. The presence of electron density fluctuations in the ionosphere above seismic regions was substantiated by ample satellite data [32]. Changes in the ionic composition and temperature of the plasma in the upper ionosphere and perturbations of the height profile of the ionospheric F region were recorded [33, 34]. An analysis of satellite photographs of the Earth's surface in the infrared (IR) frequency range showed the presence of stable and unstable components of the anomalous IR radiation flux above active crust faults; this flux corresponded to an increase in the temperature of the near-Earth layer by several degrees [35–38]. In addition, seismic activity

growth caused the appearance of anomalous airglows at 557.7 and 630 nm [39]. Immediately before earthquakes, optical phenomena in the form of lightning flashes and glows were observed [40]. Simultaneously with electromagnetic and plasma phenomena in the ionosphere, an increase in the concentration of certain gases (e.g., H_2 , CO_2 , and CH_4) by several orders of magnitude, an increase in atmospheric radioactivity (related to such radioactive elements as radon, radium, uranium, thorium, and actinium and their decay products), and an increase in the injection of soil aerosols were observed [41–45]. The influence of dynamic processes in the lower atmosphere on the ionosphere was substantiated by satellite observations of electric field perturbations and plasma density fluctuations above typhoon development regions [46, 47].

A joint analysis of observation results led us to conclude that seismic and meteorological activity stimulates the development of intense processes in the lower atmosphere. Seismic waves, chemically active and radioactive substances, and charged aerosols act simultaneously on the lower atmosphere. Heating of the lower atmosphere, sharp changes in its electrophysical parameters, the generation of acoustic waves, and the formation of extraneous electric currents occur. The acoustic action on the ionosphere appears because of the propagation upward of infrasonic waves [48]. Processes in the lower atmosphere (seismic waves, atmosphere heating, and the injection of gases) result in the generation and propagation upward of internal gravity waves, which perturb the ionosphere [49]. The formation of ultralow-frequency radiation on the Earth's surface by lithospheric sources is considered in [50, 51], along with the possibility of its penetration into the ionosphere, in [52]. Numerous studies of the nature of atmosphere–ionosphere interactions aimed at determining their mechanism have been performed. For instance, the physical processes of formation of currents in the lithosphere and propagation of their radiation into the ionosphere were considered in [52–54]. In [55–57], acoustic actions resulting in ionospheric perturbations and the generation of geomagnetic pulsations were discussed. One of the important problems of atmosphere–ionosphere interactions is the search for a chain of processes related to acting factors and identification of a set of observed effects of a common nature. This approach was applied to construct the electrodynamic model of the action on the ionosphere. The electric field near the Earth's surface experiences substantial changes days or weeks before an earthquake. The possibility of predicting earthquakes by recording an increase in conductivity and a decrease in the electric field in the atmosphere close to the Earth's surface caused by an increase in the concentration of radon was discussed in [28]. Estimates were made based on the simple model of changes in the conduction of an atmospheric column. Several possible mechanisms of atmospheric electric field strengthening before an earthquake were discussed in [58]. Ionosphere modification

was shown to be related to an increase in the injection of radon and metallic aerosols in the region of the seismic focus [59]. The mechanisms of penetration of electric fields into the ionosphere and perturbation of its electrophysical parameters were analyzed in [60–62].

The electrodynamic model is based on the assumption that the ionosphere is influenced by changes in the electric current in the closed atmosphere–ionosphere circuit. The electric current that flows from the ionosphere to the Earth's surface is a closed circuit portion with electromotive force locations in regions with thunderstorm activity [63]. Current in the closed circuit changes because of the appearance of additional extraneous currents and load resistance variations. Extraneous currents and the main load resistance (~80%) are concentrated in the near-Earth atmospheric layer several km high. It is this layer where the most intense hydrodynamic, thermodynamic, chemical, and other processes occur. These processes change the electrophysical parameters of the atmosphere and cause the formation of an extraneous electric current. For this reason, current in the closed circuit is most sensitive to changes in the characteristics of the lower atmosphere [64–68]. It follows that current changes are responsible for electrodynamic relation between the lower atmosphere and ionosphere. This stimulates plasma and electromagnetic processes in the ionosphere observed by satellites [14, 68–72]. Local perturbations close to the Earth's surface have no substantial influence on ionospheric currents. Significant changes appear when the lower atmosphere conduction level varies or vertical extraneous current forms simultaneously over regions with horizontal scales comparable with the height of the lower ionosphere boundary. The characteristic time of such changes must be on the order of or longer than the time of the establishment of this conduction level by atmospheric processes over such a horizontal scale.

The electrodynamic action of seismic and meteorological processes on the ionosphere depends on changes in the electric current value in the global atmosphere–ionosphere circuit [47, 66, 73–75]. Its source is extraneous electric current formed as a result of the convective transfer upward of charged aerosols in the lower atmosphere. In regions of typhoon development, atmospheric aqueous and salt aerosols are transferred. In regions of crust faults, aerosols are injected into the atmosphere with soil gases. The intensity of injection sharply increases as seismic activity grows before earthquakes and volcanic eruptions. Calculations show that the electric field of the current that flows in the ionosphere can reach values of 10 mV/m observed on satellites. Electric field strengthening in the ionosphere stimulates the development of plasma and electromagnetic effects recorded by satellites [68]. The instability of acoustic-gravitational waves in the lower ionosphere develops. This results in the formation of horizontal conduction inhomogeneities, the generation of longitudinal currents into the magnetosphere, and the formation of plasma layers in it [69]. When a satellite

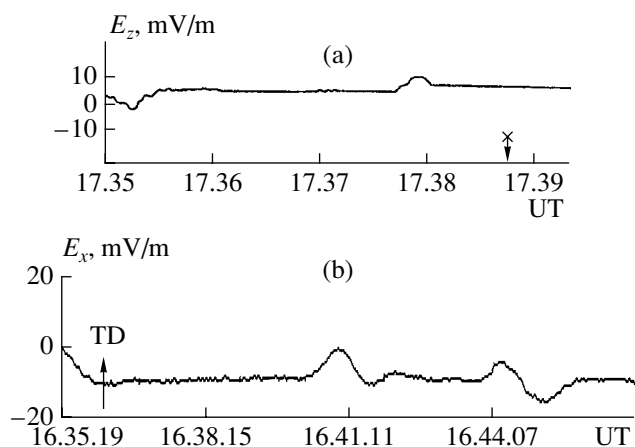


Fig. 1. Electric field measurements on (a) the Interkosmos-Bolgariya 1300 satellite above the forthcoming earthquake epicenter and (b) the Kosmos-1809 satellite above the WINONA typhoon.

traverses this perturbed region, plasma density fluctuations and magnetic field oscillations are recorded. The interaction of conduction inhomogeneities with electromagnetic field of lightning discharges results in the emission of extremely low-frequency radiation into the magnetosphere observed on satellites [76] and magnetic field oscillations in the ultralow-frequency range [77, 78]. Electric field strengthening in the ionosphere modifies its vertical profile related to plasma drift [79] and ionosphere heating by electric current [80]. Below, we consider the influence of the perturbation of the electrophysical characteristics of the lower atmosphere on the ionosphere. This action is caused by the dynamics of charged aerosols in seismic and meteorological activity regions. The horizontal scales of these regions are of tens and hundreds of km, and the characteristic range of process periods is from tens of hours to tens of days.

2. ELECTRIC CURRENT AND FIELD PERTURBATION IN THE ATMOSPHERE-IONOSPHERE CIRCUIT

In [68, 72], an electrodynamic model of earthquake precursors was formulated. This model allows several electromagnetic and plasma effects that arise because of electric field strengthening in the ionosphere above a seismically active region to be explained. The electric field of the ionosphere should reach a value of about 10 mV/m. Such fields were for the first time observed experimentally using satellites at low latitudes above the focus of a forthcoming earthquake [3] and above tropical typhoons [81, 82]. Examples of satellite data are shown in Fig. 1. Field measurements on the Interkosmos-Bolgariya 1300 satellite (January 12, 1982) are presented in Fig. 1a. The satellite intersected the magnetic field tube first in the southern and then in the northern hemisphere. Each magnetic tube crossing was

accompanied by an electric field burst with an amplitude of about 5–8 mV/m. The diameter of the magnetic tube cross section was of about 300 km. The earthquake occurred at 17.50.26 UT. The arrow marks the instant when the satellite flew above the epicenter [3]. Similar field bursts of a 20–25 mV/m amplitude (Fig. 1b) were observed when the Kosmos-1809 satellite flew above the WINONA typhoon on January 17, 1989. The arrow indicates the instant when the satellite crossed the typhoon epicenter latitude [46]. The relation between the atmospheric electric field and seismic activity and possible mechanisms of the penetration of the field into the ionosphere were studied in several papers [28, 33, 58, 83]. The calculations performed in these works showed that the field in the ionosphere reached a value of 0.1–1.0 mV/m if its vertical component on the Earth's surface was above 1–10 kV/m simultaneously over a horizontal scale of from tens to hundreds of km. The data of surface measurements of the vertical electric field component before earthquakes are evidence that the duration of electric field bursts with several kV/m amplitudes is 1–3 h, and these bursts are likely fairly local in character [31]. According to these data, field bursts with a 0.5 kV/m amplitude and a 1–2 h period were observed 8–10 h before earthquakes. Ionospheric precursors are observed during several days or tens of days [19]. For this reason, such field bursts cannot be the source of ionospheric precursors. Field changes with periods of a day or longer have amplitudes not exceeding 100 V/m. The identification of field changes with periods of several days, however, requires data collected during a large time interval to be analyzed. Experimental data lead us to the following conclusions. Field strengthening in the ionosphere to values on the order of 10 mV/m over a period of several days or tens of days is related to changes in its vertical component on the Earth's surface by no more than 100 V/m. A model of electric field perturbation by conduction currents in the atmosphere and ionosphere was considered in [47, 73]. The source of these conduction currents was an extraneous electric current. It appeared because of the injection of charged aerosols into the atmosphere with soil gases, the transfer of these aerosols upward, and their gravitational sedimentation with charge relaxation. It follows that the time scales of extraneous current variations and the injection of soil gases into the atmosphere should coincide. Strengthening of the injection of gases and accompanying elements into the atmosphere is observed during several days or even weeks before an earthquake. Estimates of the electric field in the ionosphere obtained using this model give values on the order of 10 mV/m.

2.1. Equations Describing the Electric Potential in the Ionosphere

Let us consider the generation of an electric field perturbation by an extraneous current \mathbf{j}_e in the Earth-ionosphere layer. We wish to obtain a system of equa-

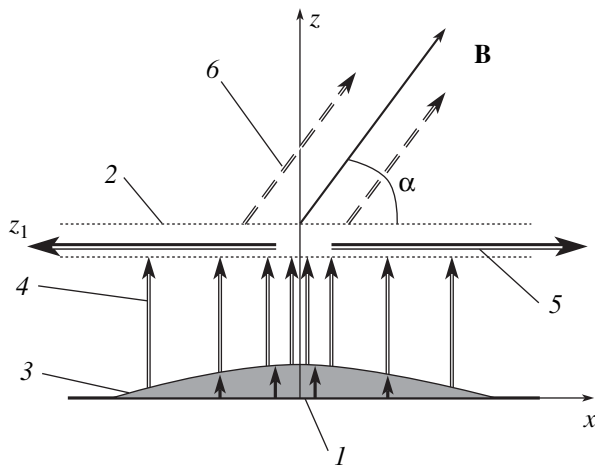


Fig. 2. Scheme of an atmosphere-ionosphere electric circuit portion: (1) Earth's surface, (2) conducting ionosphere layer, (3) extraneous electric currents, (4) conduction currents in the atmosphere, (5) conduction currents in the ionosphere, and (6) field-aligned current.

tions that determine the potential φ of electric field perturbation $\mathbf{E} = -\nabla\varphi$. For this purpose, we introduce Cartesian coordinates (x, y, z) with the z axis directed vertically upward, as is shown in Fig. 2. The homogeneous magnetic field \mathbf{B} is directed at the angle α with respect to the x axis. The $z = 0$ plane coincides with the ideally conducting Earth's surface. We assume that the electric field potential is zero on this plane, $\varphi|_{z=0} = 0$. The layer $0 < z < z_1$ is the atmosphere, whose conductivity $\sigma(z)$ depends on the altitude z . The $z = z_1$ plane coincides with the thin conducting ionosphere characterized by the integral conductivity tensor with the components Σ_P and Σ_H (the Pedersen and Hall conductivities, respectively). For slow processes with characteristic times $t \gg 1/\sigma$, the potential φ is found from the current continuity equation and the Ohm law,

$$\nabla(\mathbf{j} + \mathbf{j}_e) = 0, \quad \mathbf{j} = \sigma\mathbf{E} = -\sigma\nabla\varphi.$$

The formation of an extraneous current in the atmosphere is related to turbulent transfer upward of charged aerosols injected from the soil into the atmosphere, their gravitational sedimentation, and neutralization. Strengthening of seismic or meteorological activity increases the injection of aerosols into the atmosphere together with soil gases and their transfer in the lower atmosphere. These processes cover regions with the horizontal scale r_0 on the order of tens or hundreds of km. Let h be the spatial scale of conductivity changes in the atmosphere. At $r_0 \gg h$, we then find from the equations given above that

$$\frac{d}{dz} \left[\sigma(z) \frac{d\varphi(\mathbf{r}, z)}{dz} - j_e(\mathbf{r}, z) \right] = 0 \quad (2.1)$$

for such processes. Here, \mathbf{r} is the radius vector in the (x, y) plane.

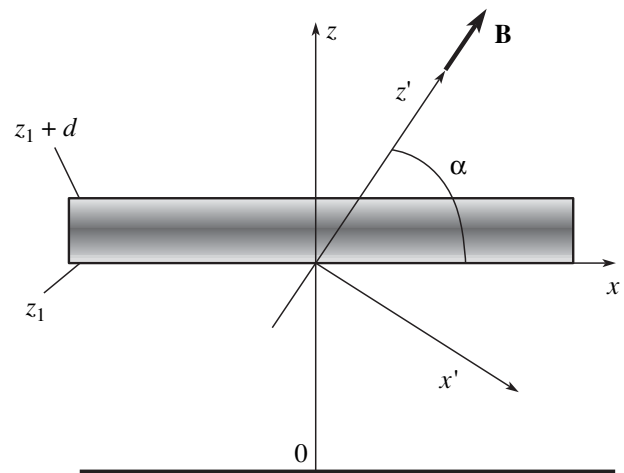


Fig. 3. Coordinate systems used to derive boundary conditions.

Let us obtain the boundary conditions for the potential φ on the $z = z_1$ plane, which coincides with the thin conducting ionosphere. The potential of electric field perturbation in the ionosphere is found from the continuity equation and generalized Ohm law,

$$\nabla\mathbf{j} = 0, \quad \mathbf{j} = \hat{\sigma}\mathbf{E} = -\hat{\sigma}\nabla\varphi,$$

where $\hat{\sigma}(z)$ is the conductivity tensor of the ionosphere. In the approximation of a stratoinhomogeneous medium, this tensor is assumed to depend on the height z above the Earth's surface only. Let us introduce auxiliary coordinates (x', y', z') with the z' axis directed along the geomagnetic field \mathbf{B} (see Fig. 3),

$$x' = x \sin \alpha - z \cos \alpha, \quad y' = y, \quad z' = x \cos \alpha + z \sin \alpha.$$

In these coordinates, the conductivity tensor takes the form

$$\hat{\sigma} = \begin{pmatrix} \sigma_P & \sigma_H & 0 \\ -\sigma_H & \sigma_P & 0 \\ 0 & 0 & \sigma_{\parallel} \end{pmatrix},$$

and the potential φ satisfies the equation

$$\begin{aligned} & \frac{\partial}{\partial z'} \left(\sigma_{\parallel} \frac{\partial \varphi}{\partial z'} \right) + \sigma_P(z) \Delta'_{\perp} \varphi \\ & - \frac{d\sigma_P}{dz} \cos \alpha \frac{d\varphi}{dx'} + \frac{d\sigma_H}{dz} \cos \alpha \frac{d\varphi}{dy'} = 0, \\ & z = z' \sin \alpha - x' \cos \alpha, \end{aligned}$$

where Δ'_{\perp} is the Laplace operator with respect to the (x', y') coordinates. The inequality $\sigma_{\parallel} \gg \sigma_P, \sigma_H$ holds in the ionosphere at $z > 80$ km. The passage to the $\sigma_{\parallel} \rightarrow \infty$ limit yields

$$\frac{\partial \varphi}{\partial z'} = 0,$$

$$\frac{\partial j_{\parallel}}{\partial z'} = \sigma_P(z) \Delta'_{\perp} \varphi - \frac{d\sigma_P}{dz} \cos \alpha \frac{d\varphi}{dx'} + \frac{d\sigma_H}{dz} \cos \alpha \frac{d\varphi}{dy'},$$

$$z = z' \sin \alpha - x' \cos \alpha,$$

where j_{\parallel} is the longitudinal current flowing in the magnetosphere between conjugated ionosphere regions. The first equation is the condition that geomagnetic field lines be equipotential, and the φ potential is therefore independent of z' . The second equation determines longitudinal current changes caused by its spreading over the ionosphere. Let us integrate the second equation along the geomagnetic field line over z' from the lower ionosphere boundary ($z = z_1$, $z' = z_1 + x \cos \alpha$) to its upper boundary ($z = z_1 + d$, $z' = z_1 + d \sin \alpha + x \cos \alpha$) at constant x' and y' . We assume that $\sigma_P = \sigma_H = 0$ at the upper and lower ionosphere boundaries. The integration yields

$$j_{\parallel}(z_1 + d \sin \alpha + x \cos \alpha) - j_{\parallel}(z_1 + x \cos \alpha) = \Delta'_{\perp} \varphi \int_0^d \sigma_P(z) \frac{dz'}{dz} dz, \quad \frac{dz'}{dz} = \frac{1}{\sin \alpha}.$$

In the (x, y, z) coordinates, this equality takes the form

$$j_{\parallel}(x + d \cot \alpha, y, z_1 + d) - j_{\parallel}(x, y, z_1) = \frac{\Sigma_P}{\sin \alpha} \left(\frac{1}{\sin^2 \alpha} \frac{\partial^2 \varphi}{\partial x^2} + \frac{\partial^2 \varphi}{\partial y^2} \right),$$

where $\Sigma_P = \int_0^d \sigma_P(z) dz$ is the Pedersen integral conductivity of the ionosphere. Because transverse conductivities are zero at the lower and upper ionosphere boundaries, the longitudinal current is related to the vertical current component as

$$j_{\parallel}(z = z_1) = j_{\parallel}(z = z_1 + d) = j_z / \sin \alpha.$$

If the characteristic horizontal perturbation scale ℓ is fairly large and the α angle is not too close to zero, $\ell \gg d / \tan \alpha$, we obtain the boundary condition in the "thin" ionosphere approximation (that is, as $d \rightarrow 0$) that determines the jump of the vertical electric current component in the passage through the ionosphere,

$$j_z(z_1 + 0) - j_z(z_1 - 0) = \Sigma_P \left(\frac{1}{\sin^2 \alpha} \frac{\partial^2 \varphi}{\partial x^2} + \frac{\partial^2 \varphi}{\partial y^2} \right) \Big|_{z=z_1}. \quad (2.2)$$

The other boundary condition in the thin ionosphere approximation is the potential continuity condition,

$$\varphi(z_1 + 0) - \varphi(z_1 - 0) = 0. \quad (2.3)$$

Current continuity conditions (2.2) in conjugated ionosphere regions have the form

$$j_m \sin \alpha + \sigma_1 \frac{d\varphi}{dz} \Big|_{z=z_1-0} = \Sigma_P \left(\frac{1}{\sin^2 \alpha} \frac{\partial^2 \varphi_1}{\partial x^2} + \frac{\partial^2 \varphi_1}{\partial y^2} \right),$$

$$-j_m \sin \alpha + \sigma_1 \frac{d\varphi}{dz} \Big|_{z=z_1-0} = \Sigma_P \left(\frac{1}{\sin^2 \alpha} \frac{\partial^2 \varphi_1}{\partial x^2} + \frac{\partial^2 \varphi_1}{\partial y^2} \right),$$

where j_m is the longitudinal electric current in the magnetosphere, $\varphi_1(x, y) = \varphi(x, y, z = z_1)$ is the horizontal potential distribution in the ionosphere, and $\sigma_1 = \sigma(z = z_1)$ is the conductivity of the atmosphere at the lower ionosphere boundary. The solution to (2.1) at $j_e = 0$ in the conjugated atmosphere has the form

$$\sigma_1 \frac{d\varphi}{dz} \Big|_{z=z_1-0} = \frac{\varphi_1}{\rho}, \quad \rho = \int_0^{z_1} \frac{dz}{\sigma(z)}.$$

The boundary conditions on the $z = z_1$ plane that follow from these equalities are

$$\varphi|_{z=0} = 0,$$

$$\sigma_1 \frac{d\varphi}{dz} \Big|_{z=z_1-0} = 2\Sigma_P \left(\frac{1}{\sin^2 \alpha} \frac{\partial^2 \varphi_1}{\partial x^2} + \frac{\partial^2 \varphi_1}{\partial y^2} \right) - \frac{\varphi_1}{\rho}. \quad (2.4)$$

According to the boundary condition, electric currents flow in the ionosphere in the horizontal direction. The appearance of a horizontal electric field component in the ionosphere is related to these currents. The solution to (2.1) that satisfies the $\varphi|_{z=0} = 0$ condition has the form

$$\varphi(\mathbf{r}, z) = \int_0^z \frac{j_e(\mathbf{r}, z')}{\sigma(z')} dz' - j_1(\mathbf{r}) \int_0^z \frac{dz'}{\sigma(z')}, \quad (2.5)$$

$$j_1(\mathbf{r}) = \frac{\varepsilon(\mathbf{r}) - \varphi_1(\mathbf{r})}{\rho}, \quad \varepsilon(\mathbf{r}) = \int_0^{z_1} \frac{j_e(\mathbf{r}, z)}{\sigma(z)} dz,$$

where $j_1(\mathbf{r})$ is the atmospheric conduction current at the lower ionosphere boundary. The conduction current generated by the extraneous current in the lower atmosphere flows from the atmosphere into the ionosphere. The ε and ρ values have the meaning of the electromotive force of the extraneous current and electric resistance of the atmosphere column of unit area between the Earth and ionosphere. Substituting (2.5) into boundary condition (2.4) yields an equation for determining the horizontal distribution of the ionosphere potential $\varphi_1(x, y)$. This equation has the form

$$\left(\frac{1}{\sin^2 \alpha} \frac{\partial^2 \varphi_1}{\partial x^2} + \frac{\partial^2 \varphi_1}{\partial y^2} \right) - \frac{1}{2\Sigma_P \rho} \varphi_1(\mathbf{r}) = -\frac{j_1(\mathbf{r})}{2\Sigma_P}.$$

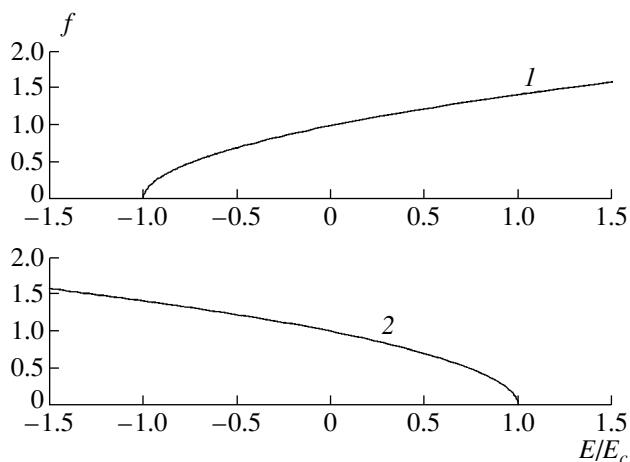


Fig. 5. Dependence of the f function on the vertical electric field component on the Earth's surface: (1) positively charged particles and (2) negatively charged particles.

vertical electric field component on the Earth's surface, namely,

$$E_{z0}(x, y) = \frac{1}{\sigma_0} [j_1(x, y) - j_p(x, y) + j_n(x, y)],$$

$$j_1(x, y) = \frac{1}{\rho} [j_p(x, y)k_p - j_n(x, y)k_n], \quad (2.11)$$

$$E_{z0}(x, y) = E_z(x, y, z = 0),$$

$$\sigma_0 = \sigma(z = 0), \quad k_{p,n} = \int_0^{z_1} dz \frac{s_{p,n}(z)}{\sigma(z)}.$$

Extraneous currents of positively and negatively charged aerosols depend on the vertical electric field component on the Earth's surface as required by the feedback mechanism,

$$j_p(x, y) = j_{p0}(x, y)f(E_{z0}(x, y)/E_{cp}),$$

$$j_n(x, y) = j_{n0}(x, y)f(-E_{z0}(x, y)/E_{cn}),$$

where $j_{p0}(x, y)$ and $j_{n0}(x, y)$ are determined by the intensity of the injection of charged aerosols without the influence of the field on them. Qualitatively, the $f(E_{z0}/E_c)$ function, which characterizes this influence, should have the form shown in Fig. 5. It follows from this figure that, after the negative field E_p reaches its critical value (E_{cp}), it blocks the flow of positively charged particles. Accordingly, a positive field blocks the flow of negatively charged particles. The critical field can be estimated in the order of magnitude from the balance equation for viscous, gravity, and electrostatic forces,

$$E_{cp} = (6\pi\eta R_p V - m_p g)/eZ_p,$$

$$E_{cn} = (6\pi\eta R_n V - m_n g)/eZ_n,$$

where η is the viscosity of air, V is the velocity of the upward movement of soil gases in earth, $R_{p,n}$ is the radius of aerosol particles, $m_{p,n} = (4/3)\pi R_{p,n}^3 \mu$ is the mass of particles, and μ is their density. The viscous force of soil gases that rise in the Earth acts on a particle in an upward direction. The gravity force is directed downward. The electrostatic force, which appears as a result of the emergence of a positively charged particle onto the surface, is directed downward. For simplicity, we assume that positively and negatively charged aerosols have equal sizes and masses, $E_{cp} = E_{cn} = E_c$. To perform calculations, let us specify the functional dependence f on electric field as $f = (1 + E_{z0}/E_c)^{1/2}$ (Fig. 4). Using this dependence in (2.11) yields

$$E_{z0}(x, y) = \frac{1}{\sigma_0} \left[j_{p0}(x, y) \left(\frac{k_p}{\rho} - 1 \right) \left(1 + \frac{E_{z0}(x, y)}{E_c} \right)^{1/2} - j_{n0}(x, y) \left(\frac{k_n}{\rho} - 1 \right) \left(1 - \frac{E_{z0}(x, y)}{E_c} \right)^{1/2} \right]. \quad (2.12)$$

Given j_{p0} and j_{n0} , this equation allows us to calculate the vertical electric field component on the Earth's surface. After solving (2.12), we can determine the horizontal distribution of the conduction current that flows from the atmosphere into the ionosphere. It follows from (2.11) and (2.12) that

$$j_1(x, y) = \frac{1}{\rho} \left[j_{p0}(x, y) \left(1 + \frac{E_{z0}(x, y)}{E_c} \right)^{1/2} k_p - j_{n0}(x, y) \left(1 - \frac{E_{z0}(x, y)}{E_c} \right)^{1/2} k_n \right]. \quad (2.13)$$

Let us consider the dependence of the electric field on the Earth's surface on the extraneous current that generates this field. We assume that the altitude dependences of extraneous currents and the conductivity of the atmosphere are described by the equations

$$s_{p,n} = \exp(-z/h_{p,n}), \quad \sigma(z) = \sigma_0 \exp(z/h),$$

where $h_{p,n}$ is the vertical scale of the spatial distribution of extraneous currents in the atmosphere. It follows from (2.11) that

$$\rho = \frac{h}{\sigma_0}, \quad k_p = \frac{hh_p}{\sigma_0(h_p + h)}, \quad k_n = \frac{hh_n}{\sigma_0(h_n + h)}.$$

Let us rewrite (2.12) in the dimensionless form

$$E_{z0} = -E_c J \left[\left(1 + \frac{E_{z0}}{E_c} \right)^{1/2} - B \left(1 - \frac{E_{z0}}{E_c} \right)^{1/2} \right],$$

$$B = \frac{\rho - k_n j_{n0}}{\rho - k_p j_{p0}}.$$

The dependence of the vertical electric field component on dimensionless current J on the Earth's surface,

$$J = j_{p0}(\rho - k_p)/\sigma_0 E_c \rho$$

$$= j_{p0} h_p / \sigma_0 E_c (h + h_p) = 0.8 j_{p0} / \sigma_0 E_c$$

is shown in Fig. 6. It follows from this figure that the vertical electric field component does not exceed

$$E_{zm} = -E_c(1 - B^2)/(1 + B^2)$$

irrespective of the current value. The calculations were performed for $j_{n0}/j_{p0} = 0.64$ and $B = (h + h_p)j_{n0}/(h + h_n)j_{p0} = 0.8$. We then obtain $E_{zm} = -0.2E_c$. Let us estimate the critical field. With $\eta = 1.72 \times 10^{-4}$ g/(cm s), $V = 0.01$ cm/s, $R = 5 \times 10^{-5}$ cm, $\mu = 1.5$ g/cm³, and $Z = 100$, the calculations give $E_c = 0.015$ CGSE = 450 V/m and $\sigma_0 E_c = 10$ nA/m². It follows that the vertical electric field component on the Earth's surface cannot exceed the value $E_{zm} = 90$ V/m.

3. THE FORMATION OF EXTRANEIOUS ELECTRIC CURRENTS

Various mechanism can be responsible for the formation of extraneous currents in the near-Earth atmospheric layer [64–66]. One of these is the intensification of the injection of charged soil aerosols into the atmosphere or changes in meteorological conditions at a stable altitude distribution of aerosols. It was mentioned in several works [41] that, several days before the main seismic impact, the concentration of metal ion-containing soil aerosols in the atmosphere can increase by one or two orders of magnitude. The quasi-stationary distribution of aerosols can be formed as a result of turbulent transfer upward and gravitational sedimentation. Turbulent transfer occurs because of a vertical horizontal wind gradient when wind kinetic energy transforms into the energy of turbulent pulsations and because of the thermal instability of the atmosphere when a negative temperature gradient exceeds its adiabatic gradient. Turbulent vortices transfer aerosols from altitudes where their concentration N is high to altitudes with a low aerosol concentration. Equilibrium is attained when the vertical flux of aerosols is balanced by their gravitational sedimentation at the rate w [84],

$$Nw = -K \frac{\partial N}{\partial z}.$$

Let us estimate the transport coefficient K of monodisperse aerosols. The rate of gravitational sedimentation is proportional to the weight mg of an aerosol particle, $w = bmg$, where m is the mass of the particle, g is the free fall acceleration, $b = 1/4\pi\eta R$ is the mobility of aerosols [85], η is the viscosity of air, and R is the radius of the aerosol particle. The data reported in [86] show that the altitude distribution of soil aerosols can be represented as $N = N_0 \exp(-z/H_a)$. It follows that the effective turbulent transport coefficient can be written

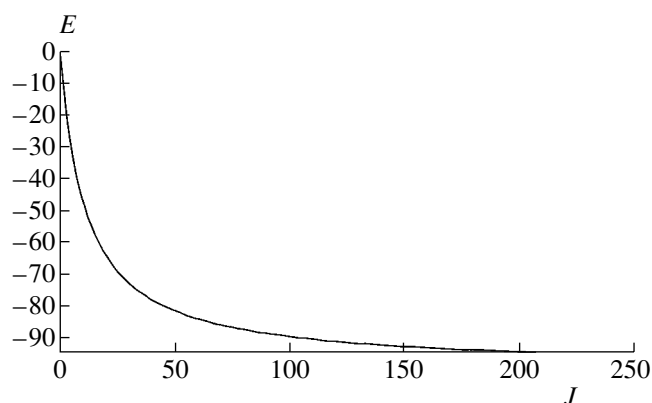


Fig. 6. Extraneous current dependence of the vertical electric field component on the Earth's surface.

in terms of the scale of the altitude distribution of soil aerosols, $K = wH_a$. Let us obtain an equation for extraneous currents formed by charged aerosols injected into the atmosphere. The charge of an aerosol particle q in the conducting atmosphere decreases with time because of charge balancing by a conduction current. The integration of the continuity equation $\partial\rho/\partial t = -\nabla\sigma E$ over the particle volume yields

$$\frac{dq}{dt} = -4\pi\sigma q.$$

The rate of the vertical transport of aerosols is the sum of the rate of gravitational sedimentation w and a random component $\xi(t)$ related to turbulent transport,

$$\frac{dz}{dt} = -w + \xi(t).$$

The method for describing the dynamics of particles determined by stochastic differential equations is based on the use of the probability distribution function [87]. We assume that some system is characterized by the "coordinates" x_i found from the equations of motion

$$\frac{dx_i}{dt} = a_i(x_i) + \xi_i(t),$$

where $\xi_i(t)$ is a random function. Assuming that

$$\langle \xi_i(t) \rangle = 0, \quad \langle \xi_i(t) \xi_k(t') \rangle = 2D_i \delta_{ik} \delta(t - t'),$$

we can obtain the Fokker–Plank equation for the probability distribution function $f(x_1, x_2, \dots, t)$ of a random process [87],

$$\frac{\partial f}{\partial t} + \sum_i \frac{\partial}{\partial x_i} (a_i f) = \sum_i \frac{\partial}{\partial x_i} \left(D_i \frac{\partial f}{\partial x_i} \right).$$

The angle brackets denote statistic averaging. Let the turbulent transport rate $\xi(t)$ satisfy the equation

$$\langle \xi(t) \rangle = 0, \quad \langle \xi(t) \xi(t') \rangle = 2K \delta(t - t').$$

We introduce the distribution function $f(q, z, t)$ of aerosol particles with respect to the electric charge and altitude. This function has the meaning of the probability that a particle has the charge q at time t and altitude z . If K weakly depends on the altitude, the kinetic equation for the f distribution function takes the form

$$\frac{\partial f}{\partial t} - w \frac{\partial f}{\partial z} - 4\pi\sigma(z) \frac{\partial}{\partial q}(qf) = K \frac{\partial^2 f}{\partial z^2}. \quad (3.1)$$

The space-time distributions of the concentration of aerosols, $N(z, t)$, their electric charge density, $\rho_e(z, t)$, and extraneous current related to their motion, $j_e(z, t)$, can be written in terms of the moments of the $f(q, z, t)$ distribution function,

$$\begin{aligned} N(z, t) &= \int_{-\infty}^{\infty} f(q, z, t) dq, \quad \rho_e(z, t) = \int_{-\infty}^{\infty} qf(q, z, t) dq, \\ j_e(z, t) &= -w \int_{-\infty}^{\infty} qf(q, z, t) dq \\ -K \int_{-\infty}^{\infty} q \frac{\partial f(q, z, t)}{\partial z} dq &= -\rho_e w - K \frac{\partial \rho_e}{\partial z}. \end{aligned} \quad (3.2)$$

The equation for the moments that follows from (3.1) and (3.2) has the form

$$\frac{\partial N}{\partial t} - w \frac{\partial N}{\partial z} = K \frac{\partial^2 N}{\partial z^2}, \quad \frac{\partial \rho_e}{\partial t} + 2\pi\sigma(z)\rho_e = -\frac{\partial j_e}{\partial z}. \quad (3.3)$$

The last equality in (3.3) is the equation

$$\frac{\partial \rho_e}{\partial t} + 4\pi\sigma\rho_e + \nabla \mathbf{j}_e = 0$$

in the one-dimensional approximation. This equation describes the density of extraneous charges and current in a conducting medium. Changes in the number of extraneous charges in a distinguished volume are determined by two processes: (1) electromotive force-induced transfer through the surface that bounds this volume and (2) a decrease in the extraneous charge caused by its relaxation into the environment with conductivity σ . For instance, if the total flux of extraneous charges through the surface bounding the volume is zero, $\nabla \mathbf{j}_e = 0$, the number of these charges in the volume decreases according to the law $\rho_e \sim \exp(-4\pi\sigma t)$. Extraneous charges relax in a conducting medium in time $\sim 1/4\pi\sigma$. If the process is fairly fast ($t \ll 1/4\pi\sigma$), charges fail to relax, and the continuity condition takes the form $\partial \rho_e / \partial t + \nabla \mathbf{j}_e = 0$. Otherwise, if extraneous charges are formed at a low rate ($t \gg 1/4\pi\sigma$), the extraneous charge density is related to the extraneous current as $4\pi\sigma\rho_e + \nabla \mathbf{j}_e = 0$. This equality means that, in the stationary state, the disappearance of extraneous charges in the volume as a result of relaxation is balanced by their transfer through the boundary surface. We assume that the char-

acteristic time of the processes under consideration is longer than the relaxation time $1/4\pi\sigma$. Equations (3.2) and (3.3) can then be used to obtain the equation that describes the altitude distribution of the extraneous current in the quasi-stationary approximation,

$$\begin{aligned} \frac{\partial}{\partial z} \left[\frac{1}{4\pi\sigma(z)} \frac{\partial j_e(z, t)}{\partial z} \right] \\ + \frac{w}{4\pi\sigma(z)K} \frac{\partial j_e(z, t)}{\partial z} - \frac{j_e(z, t)}{K} = 0. \end{aligned} \quad (3.4)$$

If the vertical scale of changes in the concentration of aerosols is smaller than the scale of conductivity changes, estimates can be obtained by (3.4) with $\sigma(z) = \sigma_0$. The solution to (3.4) then has the form

$$j_e(z, t) = j_e(0, t) \exp(-z/H_j),$$

where

$$H_j = 1/\{(w/2K) + [(w/2K)^2 + 4\pi\sigma_0/K]^{1/2}\}.$$

In the quasi-stationary approximation, the altitude extraneous charge distribution corresponding to the extraneous current has the form

$$\rho_e(z, t) = \rho_e(0, t) [\exp(-z/H_j) - H_j \delta(z)],$$

where $\delta(z)$ is the Dirac delta function. Extraneous current and charge values on the Earth's surface are determined by the equality

$$j_e(0, t) = 4\pi\sigma_0\rho_e(0, t)H_j.$$

It follows from the results obtained that extraneous currents and charges are distributed at lower altitudes than aerosols are, because charged aerosols are transported in a conducting medium and their charge relaxes. To estimate the extraneous current value, we assume that particles are injected with equal charges, $q_+ = q_- = Ze$, where Z is the number of electrons. Let the relative fraction of charged aerosols be $\lambda_{+,-} = N_{+,-}/N$. The extraneous current on the Earth's surface is determined by the concentration of aerosols,

$$j_e(0, t) = 4\pi\sigma_0 Ze(\lambda_+ - \lambda_-)H_j N(0, t). \quad (3.5)$$

It follows from (3.5) that, if $\lambda_+ > \lambda_-$, the extraneous current is directed upward. The field on the Earth's surface is directed downward.

4. ELECTRIC FIELD CALCULATION RESULTS

Let us consider electric fields generated by extraneous currents related to the dynamics of charged aerosols in the lower atmosphere. We select the large-scale axially symmetrical extraneous current distribution

$$j_e(r, z) = j_{e0} \exp\left(-\frac{z}{h_j}\right) \exp\left(-\frac{x^2 + y^2}{l^2}\right).$$

Such a current distribution corresponds to the vertical transport of aqueous aerosols in typhoon regions.

According to (2.6), the potential of the ionosphere satisfies the equation

$$\frac{1}{\sin^2 \alpha} \frac{\partial^2 \phi_1}{\partial x^2} + \frac{\partial^2 \phi_1}{\partial y^2} = -A \exp\left(-\frac{x^2 + y^2}{l^2}\right), \quad (4.1)$$

$$A = \frac{j_{e0}}{2\Sigma_p} \int_0^{z_1} \frac{\exp(-z/h_j)}{\sigma(z)} dz \left(\int_0^{z_1} \frac{dz}{\sigma(z)} \right)^{1/2}.$$

Let us pass to the dimensionless variables

$$\xi = x/l, \quad \eta = y/l, \quad \psi = -\phi_1/Al^2.$$

Equation (4.1) then takes the form

$$\frac{1}{\sin^2 \alpha} \frac{\partial^2 \psi}{\partial \xi^2} + \frac{\partial^2 \psi}{\partial \eta^2} = \exp(-\xi^2 - \eta^2).$$

The Fourier transform of the $\tilde{\psi}$ function

$$\tilde{\psi}(s, \eta) = \int_{-\infty}^{\infty} \psi(\xi, \eta) \exp(-is\xi) d\xi$$

yields

$$\frac{d^2 \tilde{\psi}}{d\eta^2} - \frac{s^2}{\sin^2 \alpha} \tilde{\psi} = \sqrt{\pi} \exp\left(-\frac{s^2}{4} - \eta^2\right).$$

The solution to this equation, which decreases as $|\xi| \rightarrow \infty$, has the form

$$\tilde{\psi}(s, \eta) = -\frac{\pi \sin \alpha}{|s|} [g(\eta, s) + g(-\eta, s)],$$

$$g(s, \eta) = \frac{1}{4} \exp\left(\frac{s^2}{4 \tan^2 \alpha} + \frac{|s|\eta}{\sin \alpha}\right) \operatorname{erfc}\left(\frac{|s|}{2 \sin \alpha} + \eta\right).$$

The spatial distribution of the dimensionless potential is determined by the inverse Fourier transform of this solution. The electric field components satisfy the equations

$$E_x = E_0 \sin \alpha \int_0^{\infty} \sin(s\xi) [g(\eta, s) + g(-\eta, s)] ds,$$

$$E_y = -E_0 \int_0^{\infty} \cos(s\xi) [g(\eta, s) - g(-\eta, s)] ds, \quad (4.2)$$

$$E_z = -E_y / \tan \alpha, \quad E_0 = j_{e0} h_j l / 2 \Sigma_p (h + h_j).$$

The horizontal electric field component in the ionosphere, $E_r(r, \varphi) = (E_x^2 + E_y^2)^{1/2}$, calculated by (4.2) for various $\varphi = \arctan(y/x)$ values is shown in Fig. 7. The $\varphi = 0$ angle corresponds to the magnetic meridian plane, and the $\varphi = \pi/2$ angle, to the transverse direction. The calculations were performed using the altitude dependence of atmosphere conductivity in the form $\sigma(z) = \sigma_0 \exp(z/h)$. We then have $A = j_{e0} h_j / 2 \Sigma_p (h + h_j)$. The extraneous current is induced because of vertical atmospheric convection, which acts as an electrostatic

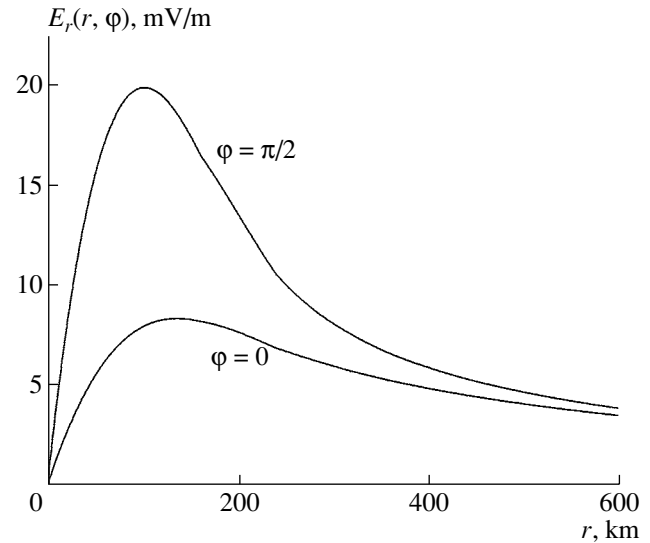


Fig. 7. Dependences of the E_r electric field component in the ionosphere on the horizontal coordinate.

generator. Air moving upward transfers small positively charged particles, whereas gravitational sedimentation transfers negative charges downward. The index of charge separation in unit cloud volume is $dQ/dt = 1 \text{ C}/(\text{km}^3 \text{ min}) \sim 10^{-11} \text{ C}/(\text{m}^3 \text{ s})$. Clearly, vertical convective movements in typhoon regions are characterized by smaller indices; their values are not known exactly. We assume that, at altitudes of $z_0 = 10 \text{ km}$, the mean charge separation index is of $\sim 4 \times 10^{-12} \text{ C}/(\text{m}^3 \text{ s})$. Estimates then give $j_{e0} \sim (dQ/dt)z_0 \sim 4 \times 10^{-6} \text{ A}/\text{m}^2$. The plots presented in Fig. 7 were calculated for $l = 100 \text{ km}$, $h = 5 \text{ km}$, $h_j = 10 \text{ km}$, $\Sigma_p = 10^{12} \text{ cm}/\text{s}$, and $\alpha = 20^\circ$. The calculation results show that the electric field component in the magnetic meridian plane is much smaller in magnitude than the component in the perpendicular plane. The horizontal distribution of the radial electric field component E_r calculated by (4.2) for the same set of parameters at various magnetic field tilt angles α is shown in Fig. 8. It follows from this figure that the distribution depends on α substantially. The spatial structure of the field has two maxima with a very small component in the magnetic meridian plane (in the center of a typhoon) when the field tilt angle is smaller than 20° .

Seismic and volcanic activity is accompanied by the injection of charged aerosols with soil gases into the atmosphere. These aerosols form extraneous electric currents. Feedback then appears between extraneous currents and the electric field on the Earth's surface. Calculations will be performed using the horizontal distribution of extraneous currents in the form

$$j_p(r) = j_{p0} \exp(-r^2/r_0^2), \quad j_n(r) = j_{n0} \exp(-r^2/r_0^2),$$

$$j_{p0} = 4\pi\sigma_0 e Z_p h_p N_{p0}, \quad j_{n0}/j_{p0} = 0.64.$$

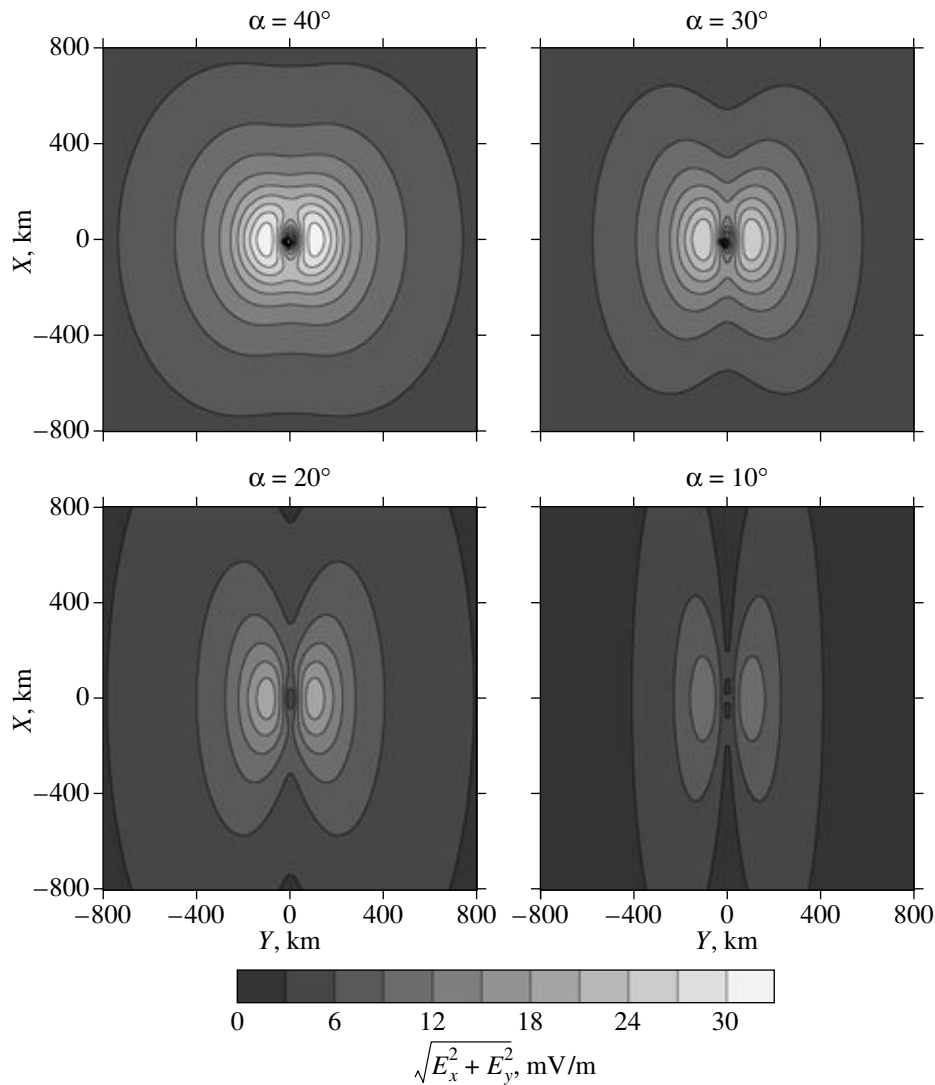


Fig. 8. Spatial distribution of the horizontal electric field component in the ionosphere at various geomagnetic field tilt angles.

The altitude dependences of extraneous currents and atmosphere conductivity are described by the equations

$$s_{p,n} = \exp(-z/h_{p,n}), \quad \sigma(z) = \sigma_0 \exp(z/h).$$

Substituting (2.13) into (2.6) yields the following equation for the horizontal electric field component in the ionosphere:

$$\left(\frac{1}{\sin^2 \alpha} \frac{\partial^2}{\partial x^2} + \frac{\partial^2}{\partial y^2} \right) \varphi_1(x, y) = -\frac{1}{2\rho \Sigma_p} \times \left[k_p j_{p0}(r) \left(1 + \frac{E_{z0}(r)}{E_{cp}} \right)^{1/2} - k_n j_{n0}(r) \left(1 - \frac{E_{z0}(r)}{E_{cn}} \right)^{1/2} \right], \quad (4.3)$$

$$E_x(x, y) = -\partial \varphi_1(x, y) / \partial x, \quad E_y(x, y) = -\partial \varphi_1(x, y) / \partial y.$$

The vertical component of the electric field in the Earth-ionosphere layer reads as

$$E_z(r, z) = \frac{1}{\sigma(z)} \left[\left(\frac{k_p}{\rho} - s_p(z) \right) j_{p0}(r) \left(1 + \frac{E_{z0}(r)}{E_{cp}} \right)^{1/2} - \left(\frac{k_n}{\rho} - s_n(z) \right) j_{n0}(r) \left(1 - \frac{E_{z0}(r)}{E_{cn}} \right)^{1/2} \right].$$

The horizontal distributions of the vertical electric field component on the Earth's surface and horizontal electric field component in the ionosphere calculated by (4.3) and (4.4) are shown in Fig. 9. The calculations were performed for $h_p = 20$ km, $h_n = 15$ km, $h = 5$ km, $r_0 = 100$ km, $N_{p0} = 8 \times 10^3$ cm⁻³, $Z_p = 100$, $\sigma_0 = 2 \times 10^{-4}$ s⁻¹, $\Sigma_p = 2 \times 10^{12}$ cm/s, and $E_c = 0.015$ CGSE = 450 V/m. It follows from Fig. 9 that the horizontal field component in the ionosphere reaches values on the order of 10 mV/m, whereas the vertical field component on the Earth's surface is no larger than 100 V/m. Calculations show that the field value on the Earth's

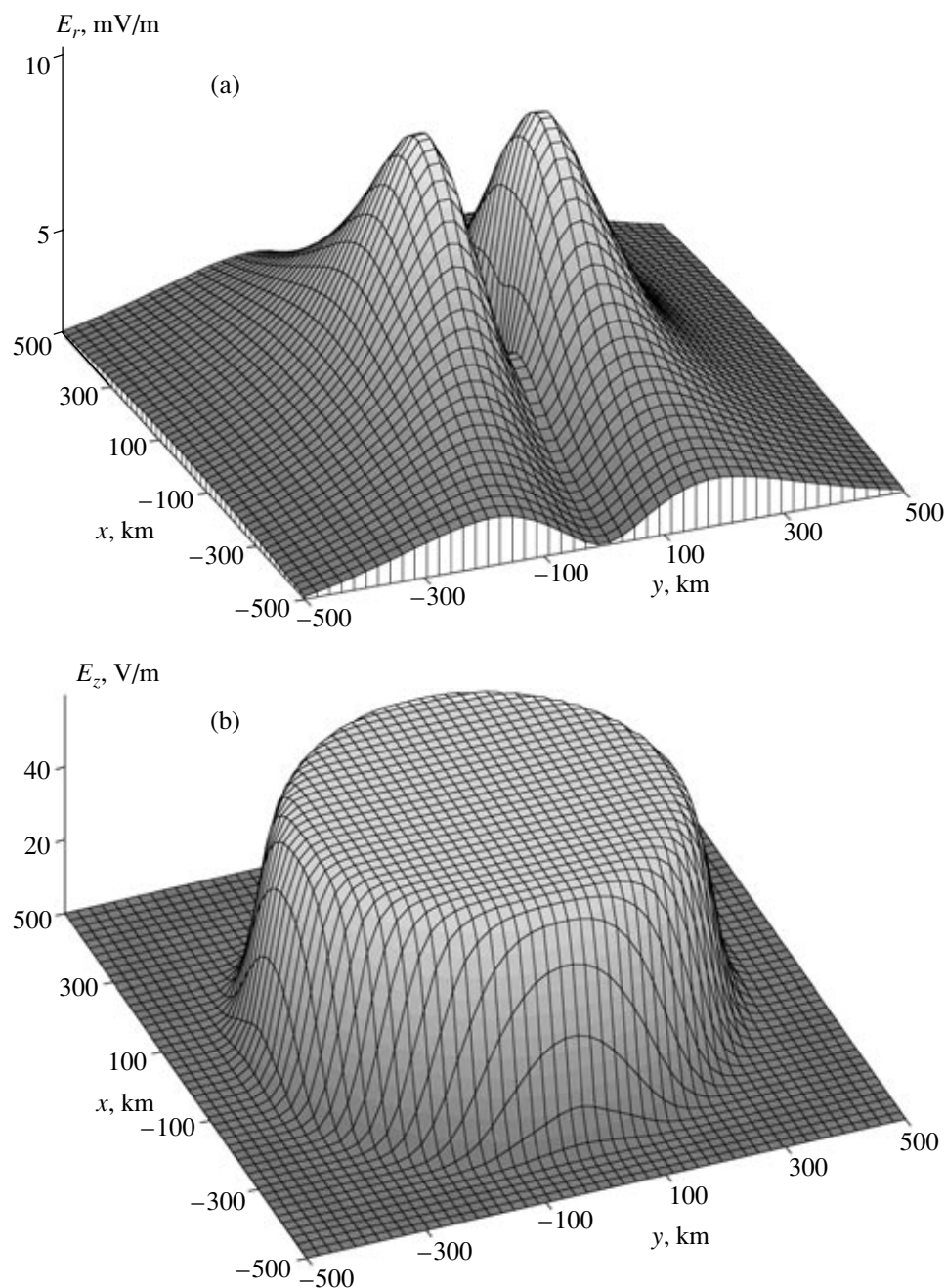


Fig. 9. Spatial distributions of the (a) horizontal electric field component in the ionosphere and (b) vertical field component on the Earth's surface.

surface is limited substantially by its feedback relation with extraneous currents. The field in the ionosphere reaches a maximum at a distance on the order of the size of the region covered by an extraneous current. The horizontal size of the region where the vertical electric field component on the Earth's surface is amplified is three times larger than the horizontal scale of the distribution of extraneous currents. Inside this region, the field virtually does not change as the distance varies.

5. PLASMA AND ELECTROMAGNETIC EFFECTS RELATED TO AN INCREASE IN ELECTRIC FIELD IN THE IONOSPHERE

Electric fields in the ionosphere above the region with intense seismic and meteorological processes appear because of the flow of conduction currents in the atmosphere-ionosphere global circuit. Their source is large-scale extraneous electric currents formed by vertical transport of charged aerosols in the lower atmosphere in the region where these processes develop.

Our calculations of electric fields are evidence that their value in the ionosphere can be as high as several dozens of mV/m units. Such fields can stimulate the development of plasma and electromagnetic effects.

5.1. Instability of Acoustic-Gravitational Waves and the Formation of Horizontal Conductivity Inhomogeneities in the Lower Ionosphere

An increase in the electric field results in the instability of acoustic-gravitational waves in the ionosphere [69, 70]. This instability is related to the transformation of the Joule heat of ionospheric currents into wave energy. It is assumed that there is strong heat exchange in a plasma, which equalizes the temperature of electrons to that of ions and molecules. Such a plasma is the commonly used model of the ionosphere with a stationary heat balance. This balance is responsible for its constant temperature. According to [88], the ionosphere can be treated as a continuous medium with a tensor conductivity in the low-frequency approximation. The propagation of small acoustic-gravitational waves in this medium is accompanied by the perturbation of conductivity and, therefore, currents. Under certain conditions, these perturbations are sufficiently strong for the Joule heat of perturbed currents to increase the amplitude of acoustic-gravitational waves. The source of energy for this instability is the electromotive force of the extraneous electric field. Field energy transforms into the energy of waves without disturbing the heat balance of the medium. The stability of acoustic-gravitational waves in an external electric field will be analyzed on the assumption that the magnetic field B is directed along the z axis, and the electric field E , along the x axis. We shall use the equations of motion, continuity, conservation, and ideal gas state in the gravitational field \mathbf{g} . The gas is characterized by the velocity \mathbf{v} , density ρ , pressure p , and temperature T ,

$$\begin{aligned}\rho d\mathbf{v}/dt &= -\nabla p + \rho\mathbf{g} + (1/c)[\mathbf{j}\mathbf{B}], \\ \partial\rho/\partial t + \nabla\rho\mathbf{v} &= 0, \\ \rho c_p dT/dt &= dp/dt + \mathbf{j}\mathbf{E}, \quad p = \rho RT.\end{aligned}$$

We shall also use the Ohm law for the current density \mathbf{j} in the ionospheric plasma,

$$\begin{aligned}\mathbf{j} &= \sigma_{\parallel}\mathbf{E}_{\parallel} + \sigma_P\mathbf{E}'_{\perp} + \sigma_H[\mathbf{B}\mathbf{E}'_{\perp}]/B, \\ \mathbf{E}'_{\perp} &= \mathbf{E} + [\mathbf{v}\mathbf{B}]/B.\end{aligned}$$

Let us consider the horizontal propagation of a plane wave along the x axis. Small velocity v_1 , density ρ_1 , pressure p_1 , and temperature T_1 perturbations with respect to their stationary values v_0 , ρ_0 , p_0 , and T_0 in the isothermal conducting exponentially inhomogeneous ionosphere satisfy the equations

$$\begin{aligned}\rho_s(\partial/\partial t + \omega_m)U &= -\partial P/\partial x, \\ \rho_s\partial W/\partial t &= -\partial P/\partial z + P/2H - gR,\end{aligned}$$

$$\partial R/\partial t + \rho_s(\partial U/\partial x + \partial W/\partial z - W/2H) = 0, \quad (5.1)$$

$$\begin{aligned}(\partial/\partial t + \omega_m)[(\partial/\partial t - \omega_2)P - a^2(\partial/\partial t + \omega_1)R \\ + (\gamma - 1)g\rho_s W] + \omega_m\omega_2 P + a^2\omega_m\omega_1 R = 0.\end{aligned}$$

Equations (5.1) contain the field variables

$$\begin{aligned}U &= (\rho_0/\rho_s)^{1/2}v_{1x}, \quad W = (\rho_0/\rho_s)^{1/2}v_{1z}, \\ P &= (\rho_0/\rho_s)^{-1/2}p_1, \\ R &= (\rho_0/\rho_s)^{-1/2}\rho_1, \quad \rho_0 = \rho_s \exp(-z/H),\end{aligned}$$

where ρ_s is the density of the atmosphere at some level corresponding to $z = 0$. The notation used in (5.1) is

$$\begin{aligned}\omega_1 &= (2\alpha + 1)(\gamma - 1)\sigma_{P0}E^2/2a^2\rho_0, \\ \omega_2 &= \gamma(\gamma - 1)\sigma_{P0}E^2/2a^2\rho_0, \\ \omega_m &= \sigma_{P0}B^2/c^2\rho_0, \quad a^2 = \gamma RT_0,\end{aligned}$$

where γ is the ratio between the specific heat capacities, R is the universal gas constant, and σ_{P0} is the Pedersen conductivity of the unperturbed ionosphere. The α coefficient characterizes the ratio between the relative changes in the density of ions and gas density in the wave. If $\alpha = 0$, conductivity perturbation is only determined by a change in the frequency of collisions depending on the density and pressure (or temperature). At $\alpha = 1$, changes in the density of ions coincide with the relative change in the density of the gas as a whole. At $\alpha > 1$, conductivity perturbation is largely determined by changes in the density of ions. In the lower atmosphere, we have $\sigma_{P0} \sim \rho_0$; the ω_1 , ω_2 , and ω_m values are therefore independent of the altitude z . The equations given above then make up a system with constant coefficients. The ω_1 value has the meaning of the ratio between the specific power of currents caused by ionosphere conductivity perturbation in an electric field and the energy density of the acoustic wave. It determines the characteristic time of external field source energy transformation into the kinetic energy of the wave. The ω_m value characterizes wave damping caused by magnetic viscosity.

Let us consider the appearance of instability for the example of the horizontal propagation of a plane wave along the x axis in a homogeneous medium, when the term containing the free fall acceleration can be ignored. We assume that the unknown values depend on the coordinates and time by the law $\exp(-i\omega t + ikx)$. The dispersion equation then takes the form

$$k^2 = \frac{\omega(\omega + i\omega_m)[\omega + i(\omega_m - \omega_2)]}{a^2[\omega + (\omega_m + \omega_1)]}. \quad (5.2)$$

The Fourier transform of the perturbation fixed in space at the initial time contains components with real wave vector values. The time dependence of perturbation is determined by complex frequencies. If $\omega = \omega' + i\Gamma$,

where $\Gamma \ll \omega'$, Eq. (5.2) yields $\omega' = ak$ and $\Gamma = -(\omega_m - \omega_1 - \omega_2)/2$. If $\omega_m > \omega_1 + \omega_2$, then $\Gamma < 0$ and the wave turns damped. At $\omega_1 = \omega_2 = 0$, the damping of the wave is determined by the parameter $\omega_m = \sigma_{p0} B^2 / c^2 \rho_0$, which characterizes induction deceleration; its value was found in [89]. If $\omega_m < \omega_1 + \omega_2$, we have $\Gamma > 0$, which corresponds to instability. The equality $\omega_m = \omega_1 + \omega_2$ determines the critical field value,

$$E_k = \frac{aB}{c} \left[\frac{2}{(\gamma - 1)(2\alpha + \gamma + 1)} \right]^{1/2}. \quad (5.3)$$

If the field is lower than critical, the initial perturbation fades out, and if it is higher, wave amplification occurs. Let us estimate E_k . Substituting $a = 3 \times 10^4$ cm/s, $B = 0.3$ Oe, $c = 3 \times 10^{10}$ cm/s, $\gamma = 1.4$, and $\alpha = 2$ into (5.3) yields $E_k = 2.6 \times 10^{-7}$ CGSE = 7–8 mV/m.

Let us consider the horizontal propagation of an acoustic-gravitational wave along the x axis on the assumption that $\partial/\partial z = 0$. Substituting the $\exp(-i\omega t + ikx)$ coordinate and time dependence of the unknown values into system (5.1) yields the dispersion equation

$$\left(\frac{ak}{\omega} \right)^2 = \frac{(\omega + i\omega_m) \{ \omega^2 [\omega + i(\omega_m - \omega_2)] - (\omega + i\omega_m) \omega_a^2 + i\omega_2 \omega_3^2 \}}{\omega \{ \omega^2 [\omega + i(\omega_m + \omega_1)] - (\omega + i\omega_m) \omega_g^2 \}}, \quad (5.4)$$

where $\omega_a^2 = \gamma g / 4H$ is the boundary acoustic frequency, $\omega_g^2 = (\gamma - 1)g / \gamma H$ is the Brunt-Váísálá frequency, and $\omega_3^2 = \omega_a^2 (2\alpha + 3) / \gamma$. At $g = 0$, (5.4) transforms into Eq. (5.2), which describes the propagation of an acoustic wave in a homogeneous medium. Let us introduce the complex refractive index $k = (n + i\kappa)\omega/c$ into (5.4). If the electric field is such that absorption can be ignored, we obtain from (5.4)

$$\begin{aligned} n(\omega) &= \frac{1}{\Omega(\omega)} \{ [A^2(\omega) + B^2(\omega)]^{1/2} + A(\omega) \}^{1/2}, \\ \kappa(\omega) &= \frac{1}{\Omega(\omega)} \{ [A^2(\omega) + B^2(\omega)]^{1/2} - A(\omega) \}^{1/2}. \end{aligned} \quad (5.5)$$

Equation (5.5) contains

$$\begin{aligned} A(\omega) &= (\omega^2 - \omega_a^2)(\omega^2 - \omega_g^2) - (\omega^2 - \omega_3^2)\omega_1\omega_2, \\ B(\omega) &= (\omega^2 - \omega_a^2)\omega\omega_1 + (\omega^2 - \omega_g^2)(\omega^2 - \omega_3^2)\omega_2/\omega, \\ \Omega(\omega) &= \{ 2[(\omega^2 - \omega_g^2)^2 + \omega^2\omega_1^2] \}^{1/2}. \end{aligned}$$

The $n = n(\omega)$ and $\kappa = \kappa(\omega)$ dependences calculated by (5.5) in the vicinity of the ω_g frequency are shown in Fig. 10. It follows from this figure that the absorption coefficient is negative and maximum in magnitude at the $\omega \sim \omega_g$ frequencies. This means that the amplitudes of waves with frequencies of about ω_g exponentially increase during wave propagation and rise above the background to produce a periodic structure. Along with density and pressure oscillations, conductivity oscillations occur in the wave. It follows that wave instability is accompanied by the formation of horizontal periodic ionosphere conductivity inhomogeneity with the scale $\ell \sim \lambda/2$, where λ is the length of the wave with an $\omega \sim \omega_g$ frequency corresponding to the extremum κ value. At these frequencies, the refractive index reaches a maximum, $n(\omega_g)$, which means a decrease in the phase wave velocity compared with the velocity of sound, $v_g = a/n(\omega_g) < a$. The horizontal conductivity inhomogeneity scale is

$$\ell = \lambda/2 = \pi v_g / \omega_g = \pi a / \omega_g n(\omega_g). \quad (5.6)$$

It follows that the instability of acoustic-gravitational waves under the action of an external electric field causes growth of plasma density perturbation and the formation of horizontal conductivity inhomogeneities with characteristic scale (5.6) in the ionosphere.

5.2. The Formation of Longitudinal Currents and Plasma Inhomogeneities in the Upper Ionosphere and Magnetosphere

Horizontal conductivity inhomogeneities change ionospheric electric fields and form plasma layers along the magnetic field [69, 70, 90]. A high conductivity along magnetic field lines results in electric field propagation into the upper ionosphere and magnetosphere. This causes the formation of an electric circuit, which includes longitudinal currents that transfer the electric field along magnetic field lines and longitudinal current-closed transverse currents caused by Pedersen conductivity. Note that longitudinal currents are carried by electrons, whereas ions are transverse current carriers. It follows that electric field propagation along magnetic field lines and the appearance of closure currents are accompanied by local changes in plasma concentration. A conductivity change in the E ionosphere layer in the presence of an extraneous electric field therefore results in the appearance of an electric polarization field. The propagation of this field into the upper ionosphere causes changes in plasma concentration at these altitudes. Whereas an acoustic-gravitational wave propagates along the x axis, conductivity inhomogeneities related to its instability are extended along the y axis. We assume that the electric field \mathbf{E}_0 is situated in the (x, y) plane and the magnetic field \mathbf{B} is directed along the z axis. When a conductivity inhomogeneity with the amplitude $\Delta\sigma_{p,H}$ moves in the E ionosphere layer in the form of an isolated band of width $\ell = \lambda/2$ extended along the y axis, plasma inhomogeneities extended along the magnetic field are formed in the upper ionosphere [91]. The horizontal velocity of band movement

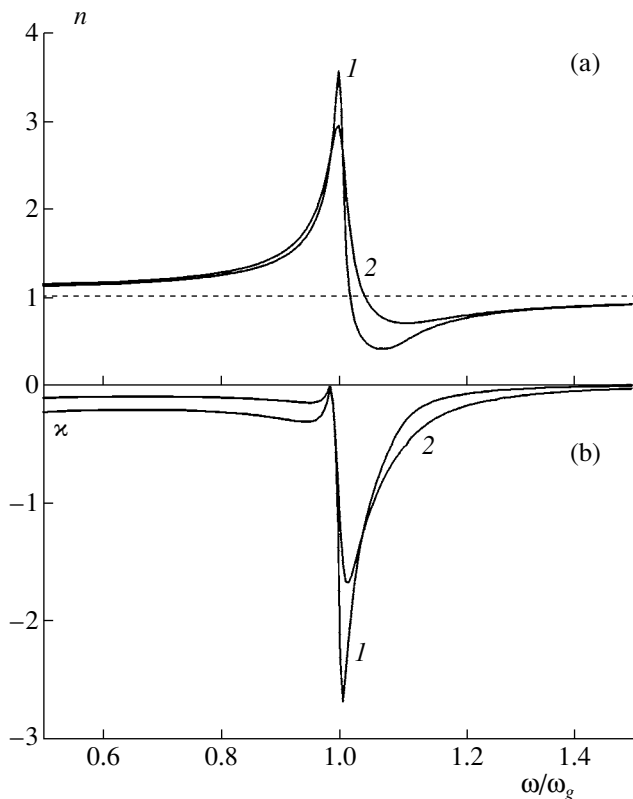


Fig. 10. Frequency dependences of the (a) refractive index n and (b) absorption index κ of the acoustic-gravitational wave propagating horizontally in an electric field. Calculations were performed for $\gamma = 1.4$, $g = 10^3$ cm/s, $H = 10^6$ cm, $\sigma_{P0} = 5 \times 10^6$ s $^{-1}$, $\rho_0 = 5 \times 10^{-13}$ g/cm 3 , $E = 3 \times 10^{-7}$ CGSE, and $\omega_g = 2 \times 10^{-2}$ s $^{-1}$. Curve 1 corresponds to $\alpha = 0.2$ ($\omega_1/\omega_g = 1.4 \times 10^{-2}$, $\omega_3/\omega_g = 2.7$), and curve 2, to $\alpha = 1$ ($\omega_1/\omega_g = 3 \times 10^{-2}$, $\omega_3/\omega_g = 3.9$).

along the x axis coincides with the velocity of the acoustic-gravitational wave and equals $v_g = a/n(\omega_g, \omega_1)$. The magnetosphere lies above the ionosphere. The magnetosphere is characterized by the Alfvén velocity v_a or wave integral conductivity $\Sigma_w = c^2/4\pi v_a$. The conducting band in the E ionosphere layer results in the appearance of the electric polarization field $\Delta\mathbf{E}$, which is transferred along magnetic field lines into the upper ionosphere and changes the plasma concentration in it. Because ions can move in a horizontal direction in an electric field, we can integrate the stationary continuity equation for ions along x at the boundary of the band to obtain $N(v_i - v_g) = N_0(v_{i0} - v_{g0})$, where n , v_i and n_0 , v_{i0} are the equilibrium concentrations and velocities of ions inside and outside the band. The velocity of ions can be determined using the equations of motion of ions and electrons,

$$\begin{aligned} M d\mathbf{v}_i/dt &= e\mathbf{E} + (e/c)[\mathbf{v}_i\mathbf{B}] - M\mathbf{v}_i\mathbf{v}_i, \\ m d\mathbf{v}_e/dt &= -e\mathbf{E} - (e/c)[\mathbf{v}_e\mathbf{B}] - m\mathbf{v}_e\mathbf{v}_e, \end{aligned}$$

where m and M are the masses of the electron and ion; v_e and v_i are the frequencies of collisions of electrons and ions; and \mathbf{v}_e and \mathbf{v}_i are the velocities of electrons and ions, respectively. In the quasi-static approximation ($\partial/\partial t = 0$), these equations yield

$$v_{ix} = v_{ex}(1 - v_i E_x / \omega_i E_{y0}) / (1 + v_i^2 / \omega_i^2),$$

where $v_{ex} = -cE_{y0}/B$ is the drift velocity of electrons and $E_x = E_{x0} + \Delta E_x$ is the electric field inside the band. The relative concentration is determined by the equation

$$\frac{N}{N_0} = \frac{(1 - v_i E_{x0} / \omega_i E_{y0}) - (1 + v_i^2 / \omega_i^2) v_g / v_{ex}}{[1 - v_i (E_{x0} + \Delta E_x) / \omega_i E_{y0}] - (1 + v_i^2 / \omega_i^2) v_g / v_{ex}}.$$

The electric polarization field of band \mathbf{E} is determined from the condition of the continuity of transverse ionospheric currents and longitudinal currents in every ionosphere layer [91],

$$E_x = \frac{\Sigma_{F0} E_{y0}}{\Sigma_P + \Sigma_w} \left[\left(1 + \frac{\Sigma_{P0} + \Sigma_w}{\Sigma_{F0}} \right) \frac{E_{x0}}{E_{y0}} + \frac{\Sigma_H - \Sigma_{H0}}{\Sigma_{F0}} \right],$$

where Σ_P and Σ_H are the integral conductivities of the lower ionosphere, Σ_w is the integral wave conductivity of the magnetosphere, and Σ_F is the integral conductivity of the upper ionosphere. This equality was obtained bearing in mind that the conductivity of the upper ionosphere was much lower than the conductivity of the E layer. The relative change in plasma concentration in the upper ionosphere above the enhanced conductivity band in the E layer is therefore determined by the equation

$$\frac{N}{N_0} = \frac{1 + D_1 - v_g / v_{ex}}{1 + D_2 - v_g / v_{ex}},$$

where

$$D_1 = v_i E_{x0} / \omega_i E_{y0}, \quad D_2 = (v_i / \omega_i) [(\Sigma_{P0} + \Sigma_w) E_{x0} / (\Sigma_P + \Sigma_w) E_{y0} + (\Sigma_H - \Sigma_{H0}) / (\Sigma_P + \Sigma_w)], \quad v_{ex} = -cE_{y0}/B.$$

We assume that the electric field is directed along the x axis; that is, $E_{y0} = 0$. The equality $\Sigma_w = \Sigma_{P0}$ holds to a fairly high accuracy in the ionosphere. If $\Delta\Sigma_P/\Sigma_{P0} = \Delta\sigma_P/\sigma_{P0}$ and $v_i c E_{x0} / \omega_i v_g B \ll 1$, the change in plasma concentration $\Delta N = N - N_0$ can be estimated by the equation

$$\frac{\Delta N}{N_0} = \frac{\Delta\sigma_P v_i c E_{x0}}{\sigma_{P0} \omega_i v_g B (2 + \Delta\sigma_P/\sigma_{P0})}.$$

This ratio tends to its limiting value

$$\frac{\Delta N}{N_0} = \frac{v_i c E_{x0}}{2\omega_i v_g B} = \frac{v_i c n(\omega_g) E_{x0}}{2\omega_i a B}. \quad (5.7)$$

as the relative conductivity perturbation $\Delta\sigma_P/\sigma_{P0}$ increases. Equation (5.7) can be used to estimate the order of magnitude of the amplitude of plasma inhomogeneities caused by the perturbation of E ionosphere level conductivity. The altitude dependence of ratio (5.7) is described by the function $v_i = v_i(z)$. It follows

that the appearance of a horizontal spatial structure of the conductivity of the ionosphere results in the formation of plasma layers extended along the geomagnetic field. The transverse size of these layers coincides with the scale of the horizontal spatial structure of conductivity.

5.3. Electromagnetic Perturbations in the Extremely Low-Frequency/Ultralow-Frequency Range

As was mentioned above, satellite data on strengthening of extremely low-frequency radiation on the eve of an earthquake were reported repeatedly. Some mechanisms of the generation of such signals have been discussed during the past years (e.g., see [11, 17]). Calculations showed that these generation mechanisms caused effects much weaker than those observed experimentally over the spectral range covering several hundred Hz. A new mechanism related to whistle-mode radiation in the upper ionosphere generated as a result of the transformation of pulsed extremely low-frequency noise on small-scale conductivity inhomogeneities in the lower ionosphere was presented in [76]. Electromagnetic pulses in the extremely low-frequency range are excited by lightning discharges and propagate in the subionosphere waveguide with weak absorption. The existence of small-scale plasma inhomogeneities was substantiated experimentally in [14, 17]. The mechanism of their formation is related to the instability of acoustic-gravitational waves as the electric field in the ionosphere increases [69, 70, 90].

The lowest eigenmode of the subionosphere waveguide (the so-called TM mode) has the weakest absorption at frequencies below 1 kHz and can therefore propagate through large distances. Because of the high conductivity of the Earth near the Earth's surface, the electric field of this mode is directed vertically. A horizontal electric field component appears as the altitude increases. Its value approaches the amplitude of the vertical component over the spectral range 100–1000 Hz at altitudes of from 115 to 120 km, at which the conductivity of the ionosphere is maximum. The horizontal electric field component induces polarization currents on conductivity inhomogeneities. These currents depend on the wave frequency and are sources of extremely low-frequency waves that propagate in the whistle mode into the upper ionosphere and magnetosphere along magnetic field lines. The horizontal Fourier components of the $E_{x,y}$ electric field of whistle waves excited by the horizontal $j_{x,y}$ polarization current components related to conductivity inhomogeneities satisfy the equation

$$\frac{\partial^2 E}{\partial z^2} + n^2 \frac{\omega^2}{c^2} E = \frac{4\pi\omega}{c^2} (j_x + i j_y),$$

where $E = E_x + iE_y$, $n = \omega_p / (\omega\omega_e)^{1/2}$ is the refractive index of whistle waves, $\omega_p = (4\pi e^2 N/m)^{1/2}$ is the plasma frequency, and $\omega_e = eB_0/mc$ is the gyrofrequency of elec-

trons. The radiating currents are determined by the perturbations of the Hall and Pedersen integral conductivities,

$$j_x = \Delta\Sigma_P E_x^0 + \Delta\Sigma_H E_y^0, \quad j_y = \Delta\Sigma_P E_y^0 - \Delta\Sigma_H E_x^0,$$

where E_x^0 and E_y^0 are the horizontal electromagnetic noise components in the waveguide. This equation can be used to find the spectral intensity of the electric E and magnetic B fields of the extremely low-frequency radiation in the upper ionosphere,

$$|E|^2 = \left(\frac{4\pi}{c}\right)^2 \frac{\omega\omega_e}{\omega_p^2} [(E_x^0)^2 + (E_y^0)^2] [(\Delta\Sigma_P)^2 + (\Delta\Sigma_H)^2], \quad (5.8)$$

$$B = nE.$$

It follows from this equation that the intensity of radiation depends on the frequency, because the horizontal electric field components in the ionosphere and the refractive index of whistle waves are frequency-dependent.

According to the data reported in several papers [8, 12, 92], an increase in electromagnetic oscillations of the noise character in the ultralow-frequency range ($f = 0.01$ – 10 Hz) can be observed in the vicinity of the epicenter of the forthcoming earthquake. According to [8], an increase in ultralow-frequency noise over the range 0.01 – 5 Hz was observed approximately 10 days before an earthquake of an $M \sim 7$ magnitude at a distance of about 50 km from the epicenter. The perturbation amplitude was of 50–100% of the mean unperturbed noise level. In [52–54], this phenomenon was explained in terms of the suggested mechanisms of the formation of sources of this radiation situated in the lithosphere and related to earthquake preparation. In [77, 78], an alternative mechanism of the generation of ultralow-frequency oscillations was presented. This mechanism should be taken into account to interpret land-based and satellite data. It involves the generation of gyrotropic waves in the lower ionosphere by a noise electromagnetic field in the presence of ionosphere conductivity horizontal inhomogeneities related to the instability of acoustic-gravitational waves caused by an increase in the electric field. These waves observed in [56] propagate in a thin lower ionosphere layer over the Earth's surface in low and medium latitudes with weak damping and at phase velocities of from tens to hundreds of km/s. Some geophysical effects related to the generation and propagation of gyrotropic waves in the horizontally homogeneous ionosphere were considered in [93–95]. A theory of these waves in the medium-latitude ionosphere was developed in [96]. Various electromagnetic radiation sources generate electromagnetic noise in the ultralow and geomagnetic pulsation frequency range. Polarization currents appear in the region of horizontal ionosphere conductivity inhomogeneities under the action of this noise. These currents are the source of gyrotropic waves. The appearance of such sources with a horizontal spatial scale of 10 km

results in the formation of narrow-band electromagnetic radiation on the Earth's surface with a characteristic frequency of about 1–10 Hz.

The suggested mechanism of the formation of narrow-band radiation can be illustrated by considering a simplified model of coherent radiation of gyrotropic waves propagating in the horizontal direction parallel with the geomagnetic field in a thin plane conducting ionosphere layer. The conductivity tensor of the ionosphere can be written as $\hat{\sigma} = \hat{\sigma}_0(z) + \hat{\sigma}_1(x, y, z)$, where $\hat{\sigma}_0$ is the conductivity tensor of the unperturbed ionosphere and $\hat{\sigma}_1$ is its perturbation, and the electric field, in the form of the sum $\mathbf{E} = \mathbf{E}_0 + \mathbf{E}_1$, where \mathbf{E}_0 is the field in the absence of conductivity perturbations ($\hat{\sigma}_1 = 0$) and \mathbf{E}_1 is the field that appears in the presence of ionosphere conductivity inhomogeneities. We assume that the perturbation is weak, $|\hat{\sigma}_1| \ll |\hat{\sigma}_0|$, and ignore second-order terms. The approximate equation for \mathbf{E}_1 then takes the form

$$[\nabla[\nabla\mathbf{E}_1]] + \frac{4\pi}{c^2}\hat{\sigma}_0\frac{\partial\mathbf{E}_1}{\partial t} = -\frac{4\pi}{c^2}\hat{\sigma}_1\frac{\partial\mathbf{E}_0}{\partial t}.$$

Let us introduce relative Hall and Pederson conductivity perturbations on the assumption that they are independent of y and z ,

$$h(x) = \sigma_{H1}(x, z)/\sigma_{H0}(z), \quad p(x) = \sigma_{P1}(x, z)/\sigma_{P0}(z).$$

In order to solve this system of equations, we shall use the model of the ionosphere in the form of two layers with different conductivity types [77]. According to this model, Pederson conductivity is nonzero in the upper layer and Hall conductivity is nonzero in the lower layer. The equations are then divided into two systems of equations each describing fields in the corresponding layers. We assume that the unknown values depend on the x coordinate and time t as $\exp(-i\omega t + ikx)$. Excluding the E_z component yields the equation for the E_y component in the layer with Hall conductivity,

$$\begin{aligned} \frac{d^2 E_{y1}}{dz^2} + \left[\left(\frac{4\pi\omega}{c^2 k} \right)^2 \sigma_{H0}^2(z) - k^2 \right] E_{y1} \\ = -2 \left(\frac{4\pi\omega}{c^2 k} \right)^2 \sigma_{H0}^2(z) f_H(k, z). \end{aligned}$$

The equation for the layer with Pedersen conductivity is obtained the same way,

$$\begin{aligned} \frac{d^2 E_{y1}}{dz^2} + \left[\frac{4\pi i\omega}{c^2} \sigma_{P0}(z) - k^2 \right] E_{y1} \\ = -\frac{4\pi i\omega}{c^2} \sigma_{P0}(z) f_P(k, z). \end{aligned}$$

In these equations,

$$\begin{aligned} f_H(k, z) &= \int_{-\infty}^{\infty} \exp(ikx) h(x) E_{y0}(x, z, \omega) dx, \\ f_P(k, z) &= \int_{-\infty}^{\infty} \exp(ikx) p(x) E_{y0}(x, z, \omega) dx. \end{aligned}$$

On the assumption that the width of the layers is much smaller than the gyrotropic wave length, we can obtain the boundary conditions for the E_y field component and its vertical derivative across the corresponding layer after integrating these equations in z . By allowing the distance between the layers to tend to zero, we obtain the boundary conditions that relate the tangent electric field component to its vertical derivative above and below the ionosphere,

$$\begin{aligned} \left\{ \frac{dE_{y1}}{dz} \right\} + \frac{1}{\ell a^2} \left[\left(\frac{\omega}{k} \right)^2 + i\omega v \right] E_{y1} \\ = -\frac{1}{\ell a^2} \left[2 \left(\frac{\omega}{k} \right)^2 f_H(k, 0) + i\omega v f_P(k, 0) \right], \end{aligned} \quad (5.9)$$

$$\{E_{y1}\} = 0.$$

Here, braces denote jumps of the corresponding values in the passage through the ionosphere. The notation used in (5.9) is as follows:

$$\begin{aligned} v &= \frac{c^2 \int_{-\infty}^{\infty} \sigma_{P0}(z) dz}{4\pi \int_{-\infty}^{\infty} \sigma_{H0}^2 dz}, \quad a = \frac{c^2}{4\pi \left(\ell \int_{-\infty}^{\infty} \sigma_{H0}^2 dz \right)^{1/2}}, \\ \ell &= \frac{\int_{-\infty}^{\infty} \sigma_{H0}^2(z) dz}{\sigma_0^2}, \end{aligned}$$

where σ_0 is the maximum Hall conductivity value. Using the solution for the electric field above and below the conducting layer and taking into account boundary conditions (5.9), we obtain

$$\begin{aligned} E_{y1}(\omega, k) &= -E_{y0}(\omega) \frac{2\omega^2 H(k)}{\omega^2 - \omega_0^2(k) + i\nu\omega k^2}, \\ H(k) &= \int_{-\infty}^{\infty} dx h(x) \exp(ikx), \end{aligned} \quad (5.10)$$

where $\omega_0^2(k) = 2\ell a^2 |k|^3$. Let us write the relative Hall conductivity perturbation in the form $h(x) = C(x) \cos k_0 x$, where the $C(x) = A \exp(-|x|/L)$ envelope changes slowly

over the scale $\lambda_0 = 2\pi/k_0$. The spatial distribution of the scattered field spectrum is obtained by applying the inverse Fourier transform with respect to k in (5.10) and taking into account the quasi-periodic character of changes in $h(x)$,

$$\frac{B_{x1}(x, \omega)}{B_{x0}(\omega)} = A \frac{(\omega/\Omega)^2}{1 + (qL)^2} \{ \exp(-|x|/L) [\sin(k_0|x|) - (qL) \cos(k_0|x|)] + i \exp[i(k_0 + q)|x|] \}, \quad (5.11)$$

$$q = (\omega^2 - \omega_0^2 + i\nu\omega k_0^2)/2\omega_0 u.$$

$$u = d\omega_0(k_0)/dk_0, \quad \Omega = (L/\omega_0 u)^{1/2},$$

Estimates show that $a = 4 \times 10^4$ m/s and $\nu = 2 \times 10^8$ m²/s. Let us calculate the relative spectrum of the amplitude of oscillations when the characteristic size of the perturbed ionosphere region, $2L$, is of hundreds of kilometers and the spatial perturbation scale $d = \lambda/2 = \pi/k_0$ is of tens of kilometers. We assume that $L = 10^5$ m, $x = 0$, and the relative Hall conductivity perturbation is $A = 0.1$. The $|B_{x1}(x, \omega)/B_{x0}(\omega)|$ relative spectrum of geomagnetic oscillation amplitude perturbations calculated by (5.11) is shown in Fig. 11. It follows from this figure that the relative perturbation is maximum in the ultralow-frequency range, and its value reaches 20–25% of the unperturbed value in the epicenter. The perturbation amplitude at the maximum decreases as the distance from the epicenter increases because of the damping of gyrotropic waves. The frequency of the perturbation spectrum maximum decreases monotonically as d increases.

The appearance of horizontal conductivity inhomogeneities in the ionosphere has a substantial influence on the characteristics of geomagnetic pulsations of magnetosphere sources in the ultralow-frequency range. These pulsations recorded on the Earth's surface appear as a result of the transformation of guided Alfvén waves into electromagnetic vibrations in the lower ionosphere when the waves propagate downward from the magnetosphere. In addition, they transform into an isotropic hydromagnetic wave, which propagates upward into the magnetosphere from the region of transformations. When horizontal conductivity inhomogeneities appear in the ionosphere, the processes of transformation and field penetration in the ionosphere change, which influences the characteristics of geomagnetic pulsations [97]. We assume that the homogeneous magnetosphere consisting of an electron-ion plasma is bounded from below by a thin conducting ionosphere. The Earth–ionosphere nonconducting layer is bounded by the plane ideally conducting Earth's surface. In Cartesian coordinates with the z axis directed downward, the homogeneous magnetic field \mathbf{B} is directed along the z axis. Let a thin conducting ionosphere layer characterized by the integral Pedersen $\Sigma_P(x, t)$ and Hall $\Sigma_H(x, t)$ conductivities,

$$\Sigma_{P,H}(x, t) = \Sigma_{P,H0} + \Delta\Sigma_{P,H}(x, t),$$

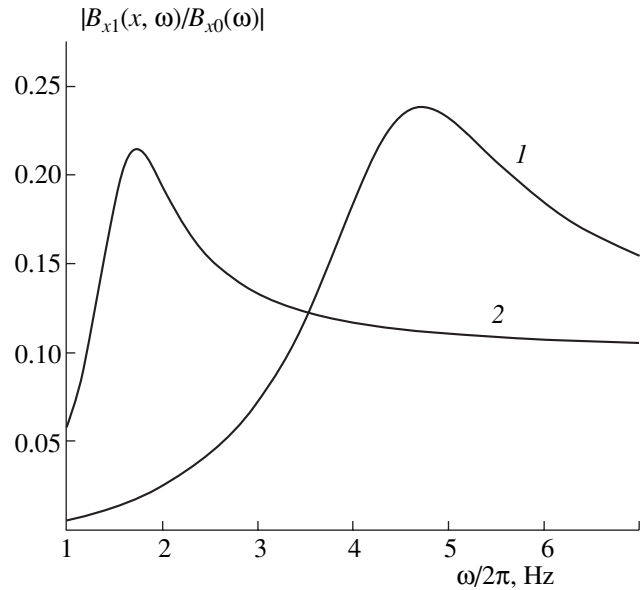


Fig. 11. Relative spectrum of the amplitude of geomagnetic oscillations constructed for different spatial scales of horizontal ionospheric conductivity inhomogeneities: $d = (1)$ 15 and (2) 30 km.

coincide with the $z = 0$ plane, and the ideally conducting Earth's surface, with the $z = h$ plane. We assume that electric field wave components are independent of the y coordinate. Because plasma conductivity along the magnetic field is high, we have $E_z \sim 0$ for the vertical field component. The electric field can be written in the form

$$\mathbf{E}(x, z, t) = \int_{-\infty}^{\infty} \frac{dk}{2\pi} \int_{-\infty}^{\infty} \frac{d\omega}{2\pi} \mathbf{E}(k, z, \omega) \exp(ikx - i\omega t).$$

The tangent electric field component is zero on the ideally conducting Earth's surface, and the jump of the tangent magnetic field component equals surface current in the ionosphere. These boundary conditions were used in [97] to obtain the integral equation for determining the horizontal electric field components in the ionosphere,

$$\hat{K}(k, \omega) \mathbf{E}(k, 0, \omega) = 2k_a \mathbf{E}_*(k) - \frac{4\pi\omega}{c^2} \int_{-\infty}^{\infty} \frac{dk'}{2\pi} \Delta \hat{\Sigma}(k - k') \mathbf{E}(k', 0, \omega), \quad (5.12)$$

where

$$\mathbf{E} = \begin{bmatrix} E_x \\ E_y \end{bmatrix}, \quad \mathbf{E}_* = \begin{bmatrix} E_* \\ 0 \end{bmatrix},$$

$$\hat{K} = \begin{bmatrix} k_1 & -k_H \\ k_H & k_2 \end{bmatrix}, \quad \Delta\hat{\Sigma} = \begin{bmatrix} \Delta\Sigma_P & -\Delta\Sigma_H \\ \Delta\Sigma_H & \Delta\Sigma_P \end{bmatrix},$$

$$k_1 = k_P + k_i + ik \cosh(kh), \quad k_2 = k_P + k_A,$$

$$k_{P,H} = 4\pi\Sigma_{P,H}\omega/c^2, \quad k_A = 4\pi\Sigma_A\omega/c^2,$$

$$\Sigma_A = c^2/4\pi u.$$

Here, $u = B_0/\sqrt{4\pi\rho}$ is the Alfvén velocity, ρ is the density of the magnetospheric plasma, and E_* is the amplitude of the incident guided Alfvén wave. The magnetic field of pulsations on the Earth's surface is calculated by the equation

$$b_x(k, h, \omega) = -i\{k/[\omega \sinh(kh)]\}E_y(k, 0, \omega). \quad (5.13)$$

Let the distribution of the amplitude of the incident guided Alfvén wave along the x coordinate be $E_*(x) = E_* \exp(ik_x x)$. Substituting the solution to (5.12) for small conductivity perturbations into (5.13) and applying the inverse Fourier transform, we obtain

$$b_{x0}(x, h, \omega) = 2E_* \frac{ick_A k_H k_x}{\omega \kappa(k_x) \sinh(k_x h)} \exp(ikx - i\omega t),$$

$$b_{x1}(x, h, \omega) = 4E_* \frac{ik_A}{c} \int_{-\infty}^{\infty} dk \frac{k \exp(ikx - i\omega t)}{\kappa(k) \sinh(kh)} \quad (5.14)$$

$$\times \{\Delta\Sigma_P(k - k_x)M_1(k_x) - \Delta\Sigma_H(k - k_x)M_2(k_x)\},$$

where

$$M_1(k) = \frac{1}{\kappa(k)} k_H [k_1(k) + k_2],$$

$$M_2(k) = \frac{1}{\kappa(k)} [k_1(k)k_2 - k_H^2], \quad \kappa(k) = k_1(k)k_2 + k_H^2.$$

The index 0 labels the unperturbed field component values, and the index 1, their perturbations.

Let us consider the influence of ionospheric perturbations on the parameters of the geomagnetic pulsations of a magnetospheric source for the example of moving conductivity inhomogeneities. According to [98], ionosphere inhomogeneities cause substantial perturbations largely of Pedersen conductivity. We can therefore leave the first term only under the integral sign in (5.14). The spatial distribution that models ionospheric conductivity perturbation will be written as

$$\Delta\Sigma_P(x) = 2\Delta\Sigma_{P0} \left[\cos \frac{k_0 x - \varphi}{2} \right]^2 \exp\left(-\frac{x^2}{4L^2}\right),$$

where $\Delta\Sigma_{P0}$ is the mean amplitude of perturbations, k_0 is the wave number of periodic perturbations, φ is their arbitrary phase, and L is the horizontal spatial scale of the perturbed region. Let us determine the relative spectral distribution of the amplitude of geomagnetic pul-

sations on the Earth's surface averaged over the period of oscillations in the form $\beta(\omega) = (\langle |b_x/b_{x0}|^2 \rangle)^{1/2}$. Equation (5.14) gives

$$\beta(\Omega) = 1 - \varepsilon \frac{f_1 f_2 + f_3^2}{f_2^2 + f_3^2},$$

$$f_{1,2} = a_{1,2}\Omega + (|\Omega^2 - \zeta_x^2|)^{1/2} \eta(\Omega - \zeta_x), \quad (5.15)$$

$$f_3 = (|\Omega^2 - \zeta_x^2|)^{1/2} \eta(\zeta_x - \Omega) + \zeta_x \coth \zeta_x$$

in the center of the perturbed region at $x = 0$. Here,

$$\varepsilon = \frac{\Delta\Sigma_{P0}}{\Sigma_A + \Sigma_{P0}}, \quad a_1 = 1 + 2 \frac{\Sigma_{P0}}{\Sigma_A},$$

$$a_2 = \frac{\Sigma_{P0}}{\Sigma_A} + \frac{\Sigma_{H0}^2}{\Sigma_A(\Sigma_{P0} + \Sigma_A)}, \quad \Sigma_A = \frac{c^2}{4\pi u},$$

$$\Omega = \frac{\omega h}{u}, \quad \zeta_x = k_x h.$$

The $\eta(x)$ function in (5.15) is the unit function, $\eta(x \geq 0) = 1$, and $\eta(x < 0) = 0$. It follows from (5.15) that $\beta(\omega = 0) = 1 - \varepsilon$, $\beta(\omega \rightarrow \infty) = 1 - \varepsilon(a_1 + 1)/(a_2 + 1)$, and $\beta(\omega)$ decreases as the frequency lowers. In the nightly ionosphere with $\Sigma_{P0} \ll \Sigma_A$, we have $\varepsilon \approx \Delta\Sigma_{P0}/\Sigma_A$, $a_1 \approx 1$, and $a_2 \ll 1$. In the daytime ionosphere with $\Sigma_{P0} \gg \Sigma_A$, $\varepsilon \ll \Delta\Sigma_{P0}/\Sigma_A$ and $a_1 \approx a_2 \gg 1$. The dependence of β on $\nu = \omega/2\pi$ calculated by (5.15) for the nightly ionosphere is shown in Fig. 12 (solid line). The following values were used in the calculations: $h = 100$ km, $\Sigma_A = 0.39$ S, $\Sigma_P = 0.43$ S, $\Sigma_H = 0.19$ S, $\Delta\Sigma_P = 0.22$ S, and the characteristic horizontal scale of changes in the incident wave field $\lambda_x = 1000$ km. For comparison, calculations for wave passage through the vertically stratified ionosphere under normal wave incidence conditions are also shown in Fig. 12 (dashed line). The frequency dependences are similar for these models. The calculated values deviate from a smooth curve in the second case because of a finite ionosphere thickness. Calculations show that the appearance of conductivity inhomogeneities in the nightly ionosphere decreases the amplitude of geomagnetic pulsations as the frequency increases, whereas, under daytime conditions, their amplitude changes insignificantly.

5.4. Perturbation of the Ionosphere

The heat flux q emitted by a thin conducting layer with the integral conductivity Σ in the horizontal electric field E equals $q = \Sigma E^2$ in the order of magnitude. With $\Sigma = 3 \times 10^{12} - 3 \times 10^{13}$ cm/s and $E = 6$ mV/m = 2×10^{-7} CGSE, we obtain $q = 0.1 - 1.0$ erg/(cm² s). One of the main sources of ionosphere heating is short-wave solar radiation ($\lambda < 1026$ Å) [99]. The supply of heat caused by the absorption of this radiation at an altitude

above 100 km is approximately several erg/(cm² s). Depending on the solar cycle, it can change several times in either direction. It follows from the estimates made above that the Joule heat of ionospheric currents in the region of earthquake preparation constitutes a substantial fraction of the total heat balance of the ionosphere. It follows that this source of heat has a determining action on the state of the ionosphere. Heating the ionosphere by currents increases the scale of the altitude distribution of the ionosphere components and, therefore, the altitude F2 layer profile. Apart from the other possible mechanisms, this mechanism should contribute to the observed ionosphere response to the processes of earthquake preparation [80].

The ionosphere is isothermal at altitudes exceeding 200 km, and there is a positive temperature gradient over the altitude range 100–200 km. Because of heat conductivity, the presence of the temperature gradient generates a heat flux directed downward. The Joule heat source is localized in the lower ionosphere layers (120–150 km). The heating of the upper ionosphere layers situated above the current layer can then only occur if gases move in the vertical direction. This effect can be estimated using a simple model of the release of the Joule heat of ionospheric currents in a thin layer coinciding with the (x, y) plane and situated at the height $z = z_1$. The magnetic field is directed along the z axis. The stationary one-dimensional movement of a gas in the plane-layered inhomogeneous ionosphere, which appears because of the action of a heat source, is then described by a system of equations of motion, continuity, heat transfer, and state,

$$\rho v \frac{dv}{dz} = -\frac{dP}{dz} - \rho g, \quad \frac{d\rho v}{dz} = 0, \quad P = k \frac{\rho T}{M},$$

$$c_p \rho v \frac{dT}{dz} = \frac{d}{dz} \left[\kappa(T) \frac{dT}{dz} \right] + q \delta(z - z_1),$$

where ρ , P , T , and v are the density, pressure, temperature, and velocity of the gas and $\delta(z - z_1)$ is the Dirac delta function. In these equations, g is the free fall acceleration, c_p is the heat capacity at a constant pressure, k is the Boltzmann constant, $\kappa(T) = \bar{v} \ell \rho c_v / 3 = \kappa_0 \sqrt{T/T_0}$ is the heat conductivity coefficient, T_0 is the temperature of the atmosphere close to the Earth's surface, $\bar{v} = (8kT/\pi M)^{1/2}$ is the mean velocity of molecules, ℓ is the free path of molecules, and c_v is the heat capacity at a constant volume. This system of equations can be used to determine the altitude temperature distribution

$$T(z) = T_0 [1 - (\sqrt{T_1/T_0} - 1)z/z_1]^2 \eta(z - z_1) + T_1 \eta(z_1 - z),$$

where $\eta(z)$ is the Heaviside unit function. The dependence of the temperature T_1 of the isothermal

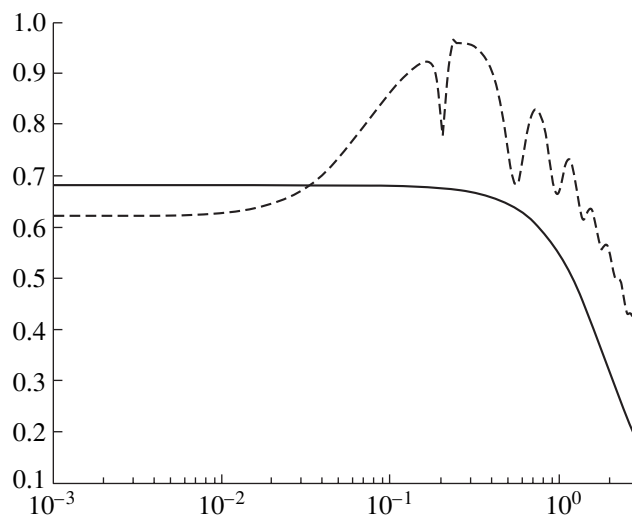


Fig. 12. Relative spectral distribution of the amplitude of geomagnetic pulsations on the Earth's surface when horizontal conductivity inhomogeneities appear in the nightly ionosphere. The solid line is the model of the oblique incidence of an Alfvén wave onto a thin conducting ionosphere layer, and the dashed curve is the model of the normal incidence of an Alfvén wave onto the ionosphere of a finite thickness.

ionosphere on the heat flux q is described by the equation

$$\frac{T_1}{T_0} \left(\sqrt{\frac{T_1}{T_0}} - 1 \right) = \frac{q}{q^*}, \quad q^* = \frac{2\kappa_0 T_0}{z_1}.$$

It follows from the continuity equation that the mass flux $I_0 = \rho v = \text{const}$ is constant and independent of z . Its dependence on the temperature T_1 of the ionosphere is determined by the equation

$$I_0 = \frac{q^*}{c_p T_0} \left(\sqrt{\frac{T_1}{T_0}} - 1 \right).$$

A gas is gradually heated as it approaches the $z = z_1$ plane where the source of heat is situated. As a result, the flux of heat transferred by the moving gas increases. At $z < z_1$, this flux is balanced by the heat flux caused by heat conductivity. At $z > z_1$, the heat flux caused by gas movement remains constant. This process characterizes heat exchange in the upper atmosphere and determines the altitude temperature distribution in it. The $q \rightarrow 0$ approximation corresponds to the transition to the isothermal atmosphere $T_1 \rightarrow T_0$, in which there is no vertical mass transfer, $I_0 = 0$. The vertical mass transfer velocity satisfies the inequality $v \ll \sqrt{gH}$, where $H = kT/Mg$. The left-hand side of the equation of motion can then be ignored, and the density can be determined using an approximate hydrostatics equation. The model of the heat balance of the ionosphere based on its heating by the vertical mass flux as a result of heat release in its lower layers can be used to

determine the temperature as a function of the heat flux. This flux is the sum of the heat released in the absorption of solar radiation predominantly in the lower ionosphere layers and the Joule heat of ionospheric currents flowing at approximately the same altitude.

Changes in the altitude distribution of ionization in the ionosphere at a given spatial electric field inhomogeneity on the Earth's surface were considered in [100]. It was assumed that the modification of the ionosphere was caused by plasma drift. As follows from the electrodynamic model, an increase in the electric current and field in the ionosphere above a seismic region and plasma drift increase the release of Joule heat. The vertical flux of neutral particles related to heat release in the lower ionosphere and an increase in the temperature of the ionosphere influence the formation of the F2 layer [80]. This influence is caused by collisions between ions and neutral particles and an increase in the vertical scale of their altitude distribution. The diffusion and photochemical processes play approximately equal roles at the layer F maximum. In its upper region, the altitude distribution of ions is largely determined by diffusion. The relation between the velocities of ions, v_i , and molecules, v_n , is found from the stationary equations of motion

$$\begin{aligned} eNE - kTdN/dz - mNg + mNv_{ei}(v_i - v_e) \\ + mNv_{en}(v_n - v_e) &= 0, \\ -eNE - kTdN/dz - MNg - mNv_{ei}(v_i - v_e) \\ + MNv_{in}(v_n - v_i) &= 0, \end{aligned}$$

where v_{ab} is the frequency of collisions between particles a and b . As $v_e \sim v_i$, the conditions $m \ll M$ and $mNv_{en}/MNv_{in}(m/M)^{1/2} \ll 1$ yield

$$v_i = v_n - D(dN/Ndz + 1/2H),$$

where $D = 2kT/Mv_{in}$ is the ambipolar diffusion coefficient and T is the temperature of the ionosphere. This equality allows the flux of ions $G = v_iN$ to be written as

$$G = -D(dN/dz + N/2L),$$

where $L = H/(1 - v_{in}v_n/g)$. Because $v_{in} \sim \rho$ and $v_n \sim 1/\rho$, L is independent of z .

The character of F2 layer modification can be determined using the model of the daytime ionosphere [101]. According to [101], the role played by diffusion in the formation of the upper F2 layer region can be analyzed ignoring recombination. This approximation significantly simplifies calculations, but the main qualitative characteristics of the upper ionosphere remain unchanged. The concentration of ions is determined by the equation [80]

$$\begin{aligned} d^2N/dz^2 + [(2L + H)/2LH]dN/dz + N/2LH \\ + (\lambda_0/D_0)\exp[-2(z - h_0)/H] = 0, \end{aligned}$$

where λ_0 and D_0 are the ion formation function and diffusion coefficient at some altitude h_0 below the altitude of the F layer maximum. The h_0 altitude corresponds to the level where the roles played by recombination and diffusion become equal. Below h_0 , photochemical equilibrium is observed. At $z > h_0$, the solution to this equation has the form

$$N = \frac{\lambda_0}{\beta_0}U(z) - \frac{2LH(G_\infty + I_0/M)}{(2L - H)D_0}V(z),$$

where β_0 is the linear recombination coefficient at the h_0 altitude,

$$U(z) = (1 + \delta)\exp[-(z - h_0)/2L] - \delta\exp[-2(z - h_0)/H];$$

$$\delta = 2LH^2\beta_0/(4L - H)D_0;$$

$$V(z) = \exp[-(z - h_0)/2L] - \exp[-(z - h_0)/H].$$

At $z < h_0$, we have

$$N = \frac{\lambda_0}{\beta_0}\exp\left(\frac{z - h_0}{H}\right).$$

The calculated altitude profile of the F ionosphere layer is shown in Fig. 13. It follows from this figure that an increase in heat release in the lower ionosphere increases the height of the layer maximum and decreases the concentration of electrons at this altitude. The modification of the altitude distribution of the concentration of ions occurs in such a way that this concentration increases in the upper ionosphere. An increase in the concentration of $[O^+]$ atomic oxygen ions, which are the majority ions in the upper ionosphere, at these altitudes should be accompanied by an increase in the concentration of light ions. It is important for the formation of hydrogen ions that the ionization potentials of atomic oxygen and hydrogen are almost equal. This means that the resonance charge exchange reaction $O^+ + H \rightarrow H^+ + O$ occurs easily. It was for the first time shown in [102] that the distribution of the concentration of hydrogen ions $[H^+]$ in the upper ionosphere should obey photochemical equilibrium laws. The resonance recharging reaction establishes this equilibrium in such a way that the ion concentrations satisfy the equality $[H^+] = (9/8)\{[H]/[O]\}[O^+]$. This means that an increase in the concentration of atomic oxygen ions in the upper ionosphere should be accompanied by an increase in the concentration of light ions.

Along with the rearrangement of the altitude profile of the higher ionosphere above a seismically active region, we observe lower ionosphere perturbation with the formation of sporadic layers [103, 104]. The critical frequency of the sporadic E layer, f_0E_s , reaches 8–9 MHz in daytime. This value corresponds to a concentration of electrons of 10^6 cm^{-3} . High-altitude rocket measurements in the medium-latitude ionosphere showed that the concentration of electrons in the sporadic layer was $2 \times 10^5 \text{ cm}^{-3}$, and the electric field in

this layer reached 10 mV/m [105]. A model of the formation of an anomalous sporadic E layer based on the effect of the atmospheric electric current flowing into the ionosphere was considered in [106]. This current stimulates the appearance of a longitudinal current, which flows from the ionosphere into magnetosphere, and transverse current, which flows over the conducting ionosphere layer. The atmospheric current transfers ions into the ionosphere, and the longitudinal current, which balances electric charge, transfers electrons into the ionosphere. As a result, plasma concentration in the lower ionosphere increases. The ionosphere electric field in the vertical magnetic field ($\alpha = \pi/2$) is described by the equation

$$2\nabla_{\perp}[\hat{\Sigma}(x, y)\mathbf{E}(x, y)] = j_1(x, y).$$

The $j_1(x, y) = j(x, y, z = z_1)$ conduction current that flows into the ionosphere transfers positive ions moving in the atmosphere upward. The source of the conduction current is an extraneous current formed in the lower atmosphere as a result of the transfer of charged aerosols. Longitudinal current electrons move downward from magnetosphere to meet positively charged ions that move from the atmosphere. These particles increase the plasma density in the lower ionosphere. In the stationary approximation, the concentration of ions in the lower ionosphere is given by the equation

$$q - \gamma N^2 - \nabla N \mathbf{v} = 0, \quad (5.16)$$

where q is the rate of lower ionosphere ionization, γ is the recombination coefficient, and \mathbf{v} is the drift velocity of ions in the electric field. The γN^2 term in (5.16) describes particle loss in the lower ionosphere. Let us consider the equation of motion of the ions related to the $\mathbf{j}_i = eN\mathbf{v}$ horizontal ionosphere current,

$$e\mathbf{E} + \frac{e}{c}[\mathbf{v}\mathbf{B}] - M\mathbf{v}\mathbf{v} = 0,$$

where e is the charge of the electron, \mathbf{E} is the horizontal electric field component, c is the velocity of light, M is the mass of the ion, and \mathbf{v} is the frequency of collisions between ions and molecules. This equation yields the Ohm law in the form

$$\mathbf{j}_i = eN\mathbf{v} = \sigma_p\mathbf{E},$$

$$\sigma_p = gf(z)N, \quad g = e^2/M\omega_i, \quad f(z) = \beta(z)/[1 + \beta^2(z)],$$

where $\beta = \omega_i/\nu$ and $\omega_i = eB/Mc$ is the gyrofrequency of ions. Outside the perturbed region, (5.16) takes the form $q - \gamma N_0^2 = 0$. For the axially symmetrical electric current distribution in the atmosphere $j_1 = j_1(r)$, we obtain

$$E(r) \int_{z_1}^{\infty} dz f(z) N(r, z) = \frac{1}{2gr} \int_0^r r' j_1(r') dr',$$

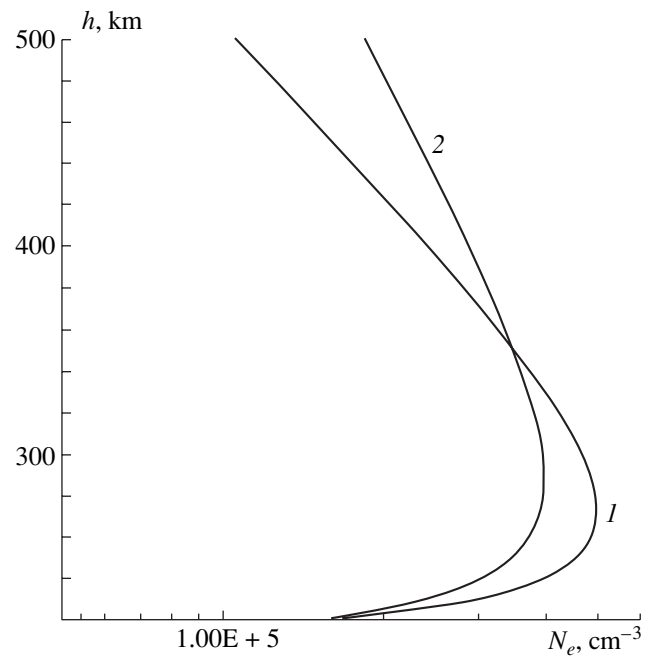


Fig. 13. Altitude profiles of the F ionosphere layer corresponding to two heat flux values released in the conducting ionosphere E layer when an electric current flows in it. Curve 1 corresponds to the unperturbed ionosphere state with an electric field of 3 mV/m, and curve 2, to the ionosphere perturbed by electric field growth up to 9 mV/m.

$$\gamma[N_0^2(z) - N^2(r, z)] \quad (5.17)$$

$$= gf(z) \left\{ E(r) \frac{\partial N(r, z)}{\partial r} + N(r, z) \left[\frac{dE(r)}{dr} + \frac{E(r)}{r} \right] \right\}.$$

Nonlinear equations (5.17) were used to calculate the spatial ion concentration and electric field distributions. The spatial electron concentration distribution for electric current flowing into the ionosphere is shown in Fig. 14. The corresponding horizontal distribution at the lower ionosphere boundary was selected to be

$$j_1(r) = j_{10} \exp(-r^2/\ell^2), \quad r^2 = x^2 + y^2.$$

The calculations [106] were performed for $j_{10} = 2 \times 10^{-6}$ A/m² and $\ell = 100$ km. The calculation results show that atmospheric electric current flowing into the ionosphere causes the appearance of a layer with an enhanced concentration of electrons in the lower ionosphere.

Note that, along with molecular ions (NO^+ , O_2^+ , O_2^{+*}), long-lived metal ions (Fe^+ , Mg^+) exist in the lower atmosphere. The concentrations of molecular ions (N), metal ions (N_1), and electrons (n) can be found using the equations

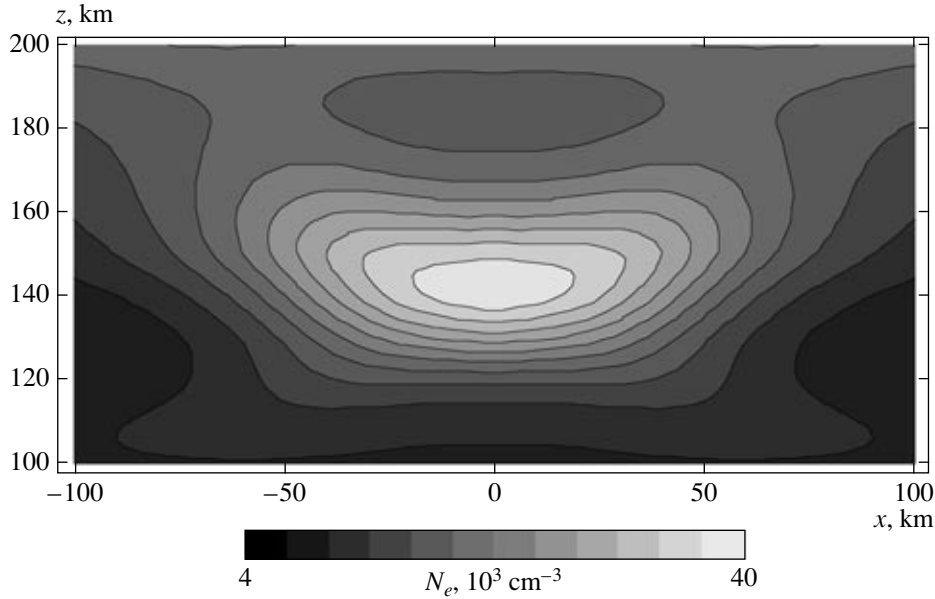


Fig. 14. Spatial distribution of the concentration of electrons in the lower ionosphere when an electric current flows into it from the atmosphere.

$$\frac{\partial N}{\partial t} + \nabla N \mathbf{v} = q - \gamma N n,$$

$$\frac{\partial N_1}{\partial t} + \nabla N_1 \mathbf{v}_1 = q_1 - \gamma_1 N_1 n, \quad n = N + N_1,$$

where q and q_1 are the effective ion formation rates and γ , γ_1 and \mathbf{v} , \mathbf{v}_1 are the recombination coefficients and velocities of molecular and metal ions, respectively. The lifetime of metal ions is much longer than the lifetime of molecular ions. This equation can therefore be simplified in the stationary approximation as

$$q - \gamma N n = 0, \quad \nabla(N_1 \mathbf{v}_1) = 0, \quad n = N + N_1. \quad (5.18)$$

The mean velocity of metal ions (\mathbf{v}_1) is found using the equation [107]

$$N_1 M_1 \frac{d\mathbf{v}_1}{dt} = N_1 e \left\{ \mathbf{E} + \frac{1}{c} [\mathbf{v}_1 \mathbf{B}] \right\} - \nabla p_1 - N_1 M_1 \mathbf{v}_1 \nu_1,$$

where M_1 and T is the mass and temperature of metal ions, ν_1 is the frequency of collisions of metal ions and molecules, and $p = N_1 k T$ (k is the Boltzmann constant). For slow processes, we have

$$\mathbf{v}_1 = \frac{\beta_1}{1 + \beta_1^2 M_1 \omega_1} \left\{ \mathbf{E}^* + \beta_1 \frac{[\mathbf{E}^* \mathbf{B}]}{B} + \beta_1^2 \frac{\mathbf{B}(\mathbf{E}^* \mathbf{B})}{B^2} \right\}, \quad (5.19)$$

$$\mathbf{E}^* = \mathbf{E} - \frac{kT \nabla N_1}{e N_1}, \quad \omega_1 = \frac{eB}{M_1 c}, \quad \beta_1(z) = \frac{\omega_1}{\nu_1(z)}.$$

in the stationary approximation. Equations (5.18) and (5.19) in conjunction with yield [106] the condition of disappearance of the longitudinal electric field in the ionosphere, $\mathbf{E} \mathbf{B} = 0$,

$$\frac{dN_1}{dz} = -p(z)N_1, \quad q - \gamma N(N + N_1) = 0,$$

$$p(z) = \frac{e}{kT} \frac{\cos \alpha}{1 + \beta^2(z) \sin^2 \alpha} \left[\frac{E_x}{\sin \alpha} + \beta(z) E_y \right].$$

A solution to this equation has the form

$$N_1(z) = N_{10} \exp \left\{ - \int_{z_1}^z p(z) dz \right\},$$

$$N(z) = - \frac{N_1(z)}{2} + \left[\left(\frac{N_1(z)}{2} \right)^2 + N_0^2(z) \right]^{1/2}, \quad (5.20)$$

$$\int_{z_1}^{\infty} N_1(z) dz = \bar{N},$$

where \bar{N} is the total content of metal ions in a column of unit cross section. This equation can be used to calculate the altitude distribution of the concentration of metal and molecular ions at a given electric field distribution in the lower ionosphere. The potential of this field $\varphi_1(x, y) = \varphi_1(x, y, z = z_1)$ satisfies the equations

$$2 \nabla_{\perp} [\hat{\Sigma}_e(x, y, \alpha) \nabla_{\perp} \varphi_1] = -j_1(x, y),$$

$$\hat{\Sigma}_e = \begin{pmatrix} \Sigma_p / \sin^2 \alpha & \Sigma_H / \sin \alpha \\ -\Sigma_H / \sin \alpha & \Sigma_p \end{pmatrix},$$

where $j_1(x, y)$ is the horizontal distribution of the conduction current flowing from the atmosphere at the

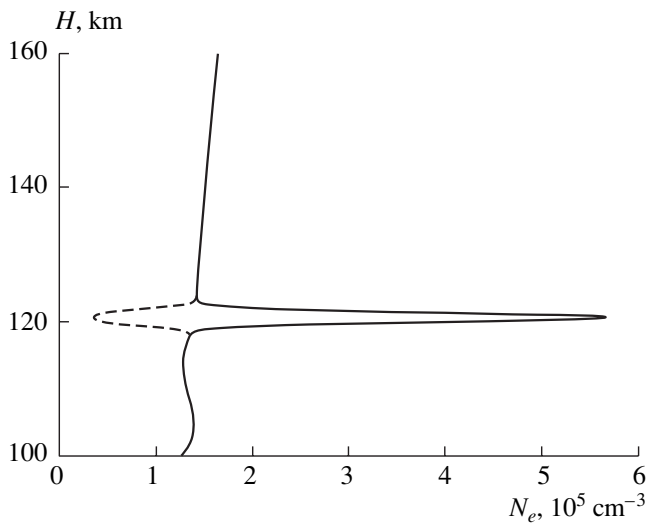


Fig. 15. Altitude distribution of the concentration of electrons in the lower ionosphere under the action of metal ions in an electric field; the dashed line is the altitude distribution of molecular ions; $\alpha = 40^\circ$.

lower ionosphere boundary. This equation is simplified in the horizontally homogeneous ionosphere,

$$\frac{1}{\sin^2 \alpha} \frac{\partial^2 \varphi_1}{\partial x^2} + \frac{\partial^2 \varphi_1}{\partial y^2} = -\frac{1}{2\Sigma_p} j_1(x, y), \quad (5.21)$$

$$\varphi(x, y, z) = \varphi[x - (z - z_1) \tan \alpha, y, z_1].$$

Equation (5.21) can be used to calculate the spatial electric field distribution in the ionosphere. The altitude distribution of the concentration of electrons calculated by (5.20) and (5.21) with the use of the IRI-90 ionosphere model is shown in Fig. 15. In Fig. 16, the calculated horizontal distribution of the

height of the electron concentration maximum is presented. It follows from the results obtained that the presence of metal ions in the lower ionosphere causes the appearance of a thin (about 3 km thick) electron concentration layer when electric current flows into the ionosphere. This layer is recorded as a sporadic *E* layer.

6. AN ELECTRODYNAMIC MODEL OF ATMOSPHERE-IONOSPHERE COUPLING

According to the electrodynamic model, an increase in the electric field in the ionosphere can be caused by an increase in the conductivity of the lower atmosphere as a result of intense radioactive substance outbursts from a seismic focus at the stage of earthquake preparation. Such outbursts have been repeatedly observed several days or weeks before the main seismic impact. The time dependence of the concentration of radon in soil gases and natural water was measured in [43]. An intense burst of radon was observed approximately a week before the earthquake. The concentration of radon then increased by factors of 2.5 and more than 1.5 in gases and water, respectively. Measurements were taken at a distance of 300 km from the epicenter. The concentration of radon was also measured in [44] (see Fig. 17). According to [44], the concentration of radon increased approximately fourfold during five days before an earthquake. It is noted in [44] that a statistical analysis of the data obtained during three years of observations for about 300 micro earthquakes ($M < 4$) in south-east Germany shows that 75% of the earthquakes were preceded by a substantial increase in the concentration of radon. It can be suggested that, simultaneously with radon, other radioactive elements are injected into the atmosphere. In addition, such injections should not necessarily be related to radon. An

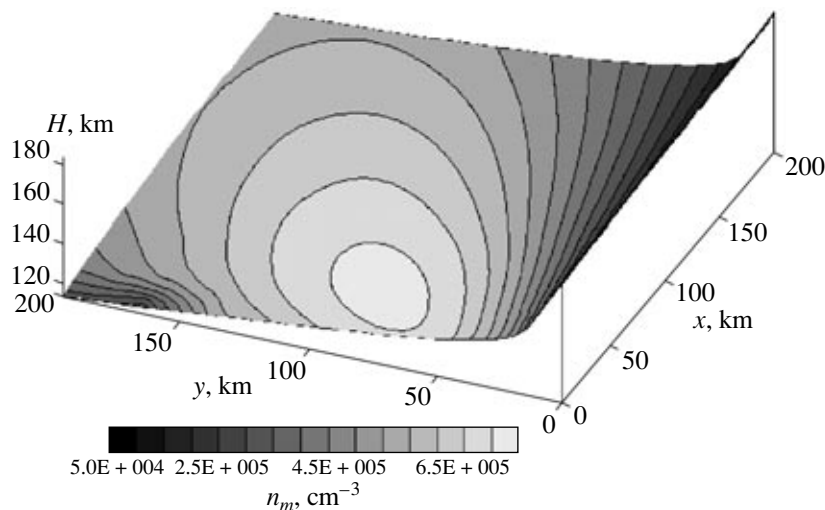


Fig. 16. Spatial distribution of the maximum of the electron concentration layer; $\alpha = 40^\circ$.

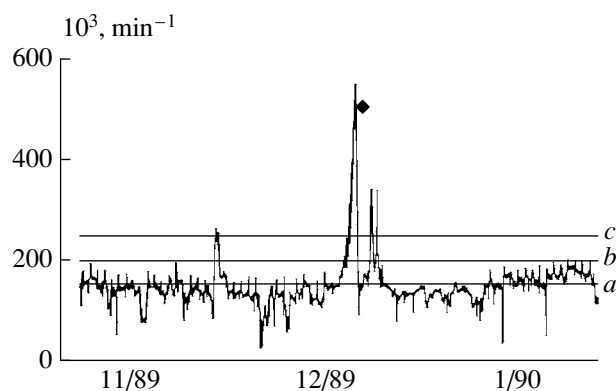


Fig. 17. Time dependence of the concentration of radon in natural water. The symbol corresponds to the earthquake instant.

increase in the concentration of soil aerosols containing metal ions in the atmosphere related to seismic activity was reported in several works [33, 41]. It follows from the model under consideration that these processes, which are responsible for extraneous currents and increase the conductivity of the lower atmosphere, cause an increase in the electric field in the ionosphere. This suggestion finds support in the data obtained in [108] after the Chernobyl accident. It was found that intense injections of radioactive substances into the atmosphere were accompanied by changes in the phase and amplitude of superlong wave signals along the propagation path crossing the accident region. The calculations performed in [109] show that such perturbations of the characteristics of the propagation of superlong wave signals can appear because of electric field growth in the ionosphere.

According to the calculations mentioned above, changes in the electrophysical state of the lower atmosphere cause an electric field increase in the ionosphere and stimulate several effects observed experimentally. An example is the satellite observations reported in [3, 14]. The data on ultralow-frequency geomagnetic field oscillations over the frequency range 0.1–8 Hz and the vertical quasi-stationary electric field E component obtained on the Interkosmos-Bolgariya 1300 satellite during 15 min before the earthquake of January 12, 1982 at 17.50.26 UT [3] are shown in Fig. 18. An increase in the electric field to 3–7 mV/m and the appearance of ultralow-frequency geomagnetic field oscillations with an amplitude of 3 nT were observed in two regions, above the epicenter and in the magnetically conjugated region. The results of extremely low-frequency/very low-frequency measurements aboard KOSMOS-1809 near Spitak showed [14] that intense extremely low-frequency radiation was generated over the longitude range $\leq 6^\circ$ and latitude range 2° – 4° about the epicenter. The intensity of radiation was about 10 pT at a 140 Hz frequency (a 25 Hz band) and about 3 pT at 450 Hz (a 75 Hz band). In the same region,

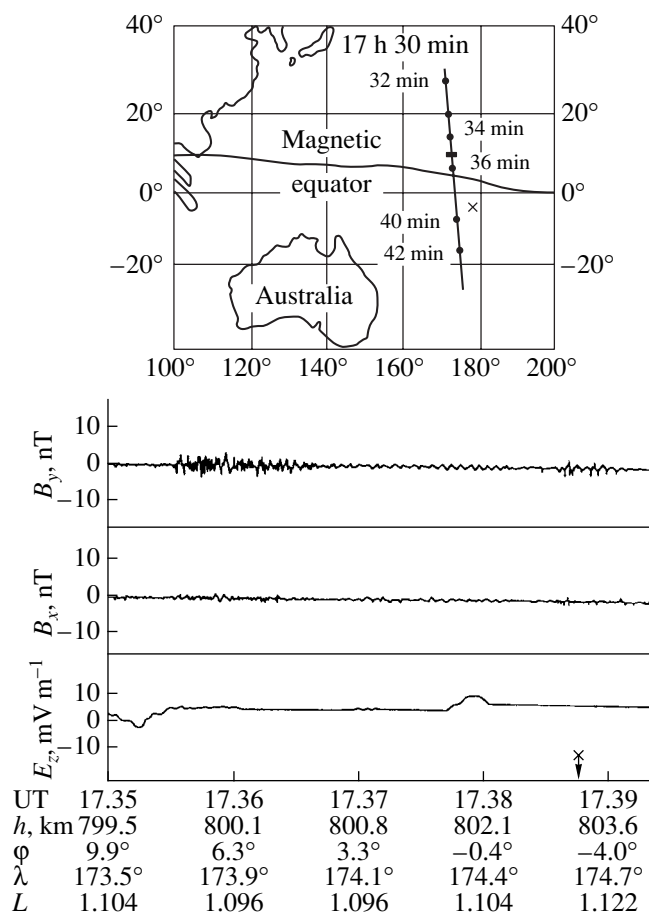


Fig. 18. Ultralow-frequency geomagnetic field oscillations and vertical quasi-stationary electric field component recorded on the Interkosmos-Bolgariya 1300 satellite. The upper part is a map of the trajectory portion over which measurements were taken.

small-scale (4 to 10 km along the orbit) plasma density inhomogeneities with the relative amplitude $\Delta N/N = 3$ – 8% were observed. These inhomogeneities were induced in the same regions as anomalous extremely low-frequency radiation. An example of such measurements is shown in Fig. 19. The existence of plasma density perturbations above seismically active regions was substantiated in [32]. An increase in the ionosphere electric field observed above the region of earthquake preparation results in the instability of acoustic-gravitational waves [69, 70]. The development of instability is accompanied by the appearance of horizontal ionosphere conductivity inhomogeneities, whose interaction with the electric field in the ionosphere is a source of radiation of guided Alfvén waves into the magnetosphere. These waves form longitudinal electric currents and plasma layers extended along the geomagnetic field. The transverse spatial size of these layers coincides with the scale of the horizontal spatial structure of conductivity. Let us consider numerical estimates. At an altitude of 1000 km, the summed frequency of ion

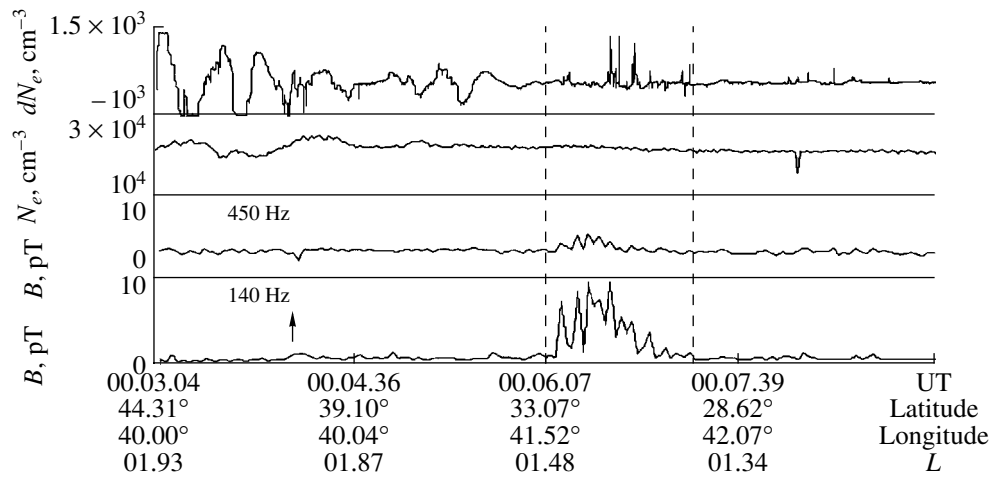


Fig. 19. Density fluctuations and extremely low-frequency radiations recorded on the Kosmos-1809 satellite on January 20, 1989. The dashed lines bound the perturbed ionosphere region. The arrow marks the instant of satellite crossing the epicenter.

collisions with ions and molecules is $v_i = v_{i(n+i)} \sim 0.5 \text{ s}^{-1}$ [110], and the gyrofrequency of ions is $\omega_i \sim 30 \text{ s}^{-1}$. For the velocity of sound $a = 3 \times 10^4 \text{ cm/s}$, perturbed electric field value $E = 9 \text{ mV/m} = 3 \times 10^7 \text{ CGSE}$, $B = 0.3 \text{ Oe}$, $n = 1-10$, and $\omega_g = 2 \times 10^{-2} \text{ s}^{-1}$, we obtain $\ell \approx \pi a / \omega_g n(\omega_g) \approx 4-40 \text{ km}$ and $\Delta N/N_0 \approx 1.6-16\%$. When a satellite moving at the velocity $v_s \sim 10^6 \text{ cm/s}$ crosses plasma inhomogeneities of horizontal scale $\ell \sim 4-40 \text{ km}$, plasma density fluctuations with the period $\Delta t = \ell/v_s = \pi a / v_s \omega_g n(\omega_g) \sim 0.4-4 \text{ s}$ are observed. Because these inhomogeneities are formed by longitudinal currents, geomagnetic oscillations with the same period are recorded when they are crossed by a satellite. Their amplitude b is $b = (\pi/c) E \Sigma_{p0} [\Delta \sigma_p / (2\sigma_{p0} + \Delta \sigma_p)] \sim 5 \text{ nT}$. These estimates are in agreement with the satellite data. To summarize, the effect of crossing longitudinal currents by a satellite moving at the velocity v_s is recorded as density fluctuations and ultralow-frequency geomagnetic field oscillations with equal periods. A scheme of such measurements is shown in Fig. 20.

Geomagnetic oscillations in this frequency range are recorded on the Earth's surface in regions of earthquake preparation [12, 93]. Along with oscillation sources that appear in seismic focus formation regions, there are sources situated in the ionosphere. These are polarization currents related to the appearance of horizontal conductivity inhomogeneities and their interaction with the background electric field. This interaction generates gyrotropic waves, which propagate in the horizontal direction and form geomagnetic oscillations in the ultralow-frequency range on the Earth's surface [77, 78]. The relative perturbation spectrum of geomagnetic oscillations is shown in Fig. 11. Relative perturbation has a maximum in the ultralow-frequency range, and its value amounts to about 40% of the unperturbed value. The frequency at the maximum decreases as the horizontal scale of inhomogeneities increases. The amplitude of perturbation at the maximum decreases as

the distance from the epicenter increases because of the damping of gyrotropic waves. The appearance of inhomogeneities in the night ionosphere causes geomagnetic pulsation depression in the ultralow-frequency range; these pulsations appear because of the incidence of guided Alfvén waves from magnetosphere sources situated above [97]. According to [76], extremely low-frequency emission in the upper ionosphere arises when pulsed electromagnetic radiation from lightning discharges propagating in the Earth-ionosphere waveguide is scattered by lower ionosphere conductivity inhomogeneities. The amplitudes of whistles in the upper ionosphere vary substantially depending on lightning activity. The magnetic field of whistles reaches a maximum of $B \approx 1-2 \text{ pT}$ over the frequency range 200–500 Hz. These characteristics correspond with the experimental data [4, 13, 14]. The estimates of the characteristic transverse size ($\sim 10 \text{ km}$) and plasma layer density inhomogeneities ($\Delta N/N_0 \sim 10\%$) obtained earlier led the authors of [111] to suggest that small-scale plasma structures excited this way could play the role of waveguides or ducts that canalized whistle waves along the external Earth's magnetic field. The ducts are plasma inhomogeneities extended along the geomagnetic field. Their transverse spatial scale is of about 10 km, and the relative change in the plasma density above the background value is of about 10%. The appearance of such structures above the epicenter region in the ionosphere increases the probability of the emergence of magnetospheric whistles into the Earth-ionosphere waveguide and changes the dispersion characteristics of signals recorded on the Earth's surface. The influence of seismic activity on the propagation of magnetospheric whistles was observed in [10]. The statistical analysis performed there showed that the characteristics of the anomalous propagation of whistles at medium latitudes, such as an increase in dispersion and appearance frequency, were consequences of seismic activity. Possible mechanisms of this influence were

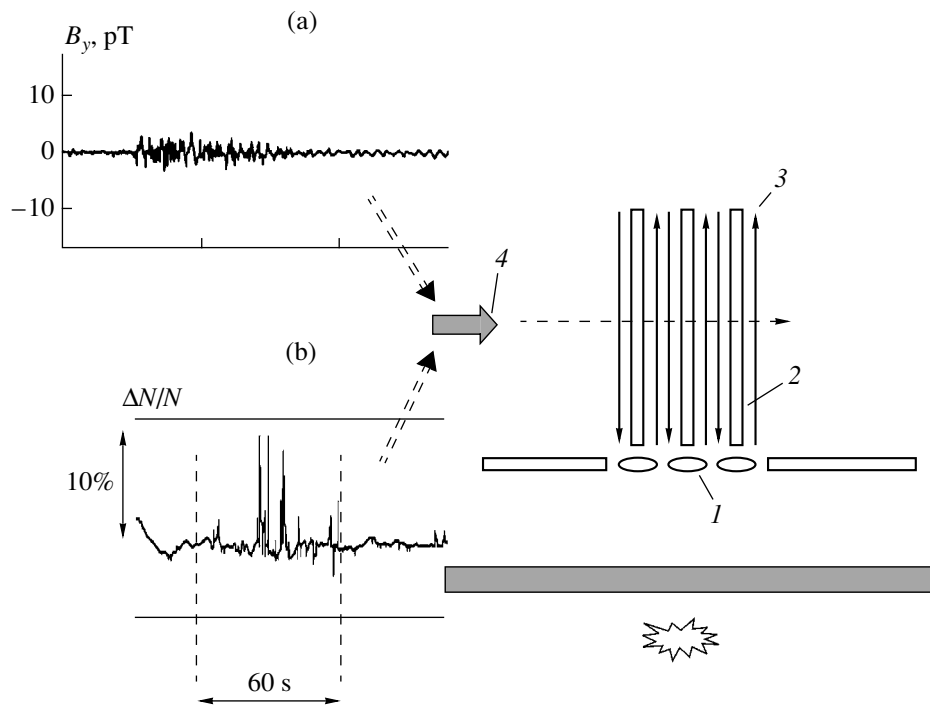


Fig. 20. Scheme of satellite observations of (a) plasma density inhomogeneities and (b) ultralow-frequency geomagnetic field oscillations: (1) horizontal ionosphere conductivity inhomogeneities, (2) plasma density inhomogeneities extended along the geomagnetic field, (3) longitudinal electric currents, and (4) satellite.

discussed in [10]. It was, in particular, suggested that seismic activity influenced the trapping of whistles in the waveguide or caused the formation of a waveguide as a result of the action of acoustic or internal gravitational waves on the ionosphere. This suggestion was substantiated experimentally [14] by satellite observations of small-scale plasma density inhomogeneities

and extremely low-frequency radiations correlated with them above seismic regions (see Fig. 19).

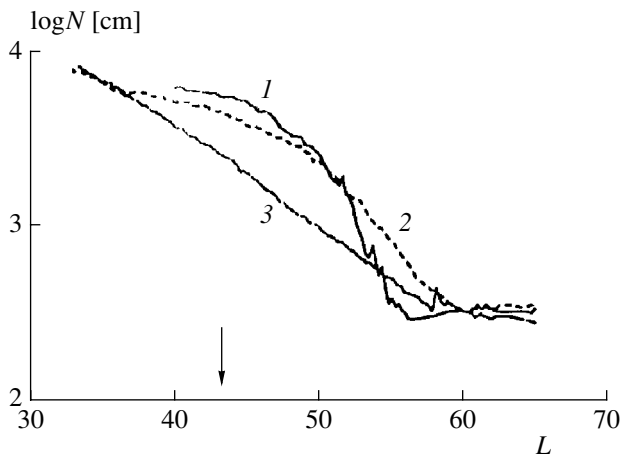


Fig. 21. The concentration of hydrogen ions measured along three Interkosmos-24 satellite orbits (L is the invariant latitude). Curves 1, 2, and 3 correspond to flights over the Asian, Mediterranean, and West European regions. The orbit altitude was 800–2400 km. The arrow indicates the instant when the satellite was closest to the epicenter in the Asian region.

At the stage of earthquake preparation, large-scale changes in the state of the ionosphere were observed several days before the main seismic impact. The data presented in [33], where the altitude electron concentration distribution in the upper part of the F2 layer was measured using a spaceborne ionoprobe (the Interkosmos-19 satellite), can serve as an example. It follows from these data that the state of the ionosphere changes substantially on the eve of an earthquake. Namely, the altitude of the F2 layer maximum increases from approximately 280 to 360 km, and the maximum electron concentration value decreases from 3×10^5 to 10^5 cm^{-3} one day before the earthquake. It was shown above that an increase in the electric field and related release of Joule heat in the lower ionosphere increased its temperature and mass flux [80]. This influenced diffusion processes that formed the F layer and changed its characteristics. By way of example, let us perform calculations using the heat flux value related to the heating of the lower ionosphere by solar radiation, $q_0 = 1 \text{ erg}/(\text{cm}^2 \text{ s})$. The integral Pedersen conductivity and the ionosphere electric field value can be set equal to $\Sigma_p = 1.4 \times 10^{13} \text{ cm/s}$ and $E_0 = 3 \text{ mV/m} = 10^{-7} \text{ CGSE}$, respectively. The heat flux is then $q = 1.14 \text{ erg}/(\text{cm}^2 \text{ s})$. Bearing in mind that $q^* = 0.2 \text{ erg}/(\text{cm}^2 \text{ s})$, we find that such a flux should heat the ionosphere to $T = 1440 \text{ K}$. Suppose that the electric field above the region of the forthcoming earthquake increases by $\Delta E = 6 \text{ mV/m} = 2 \times$

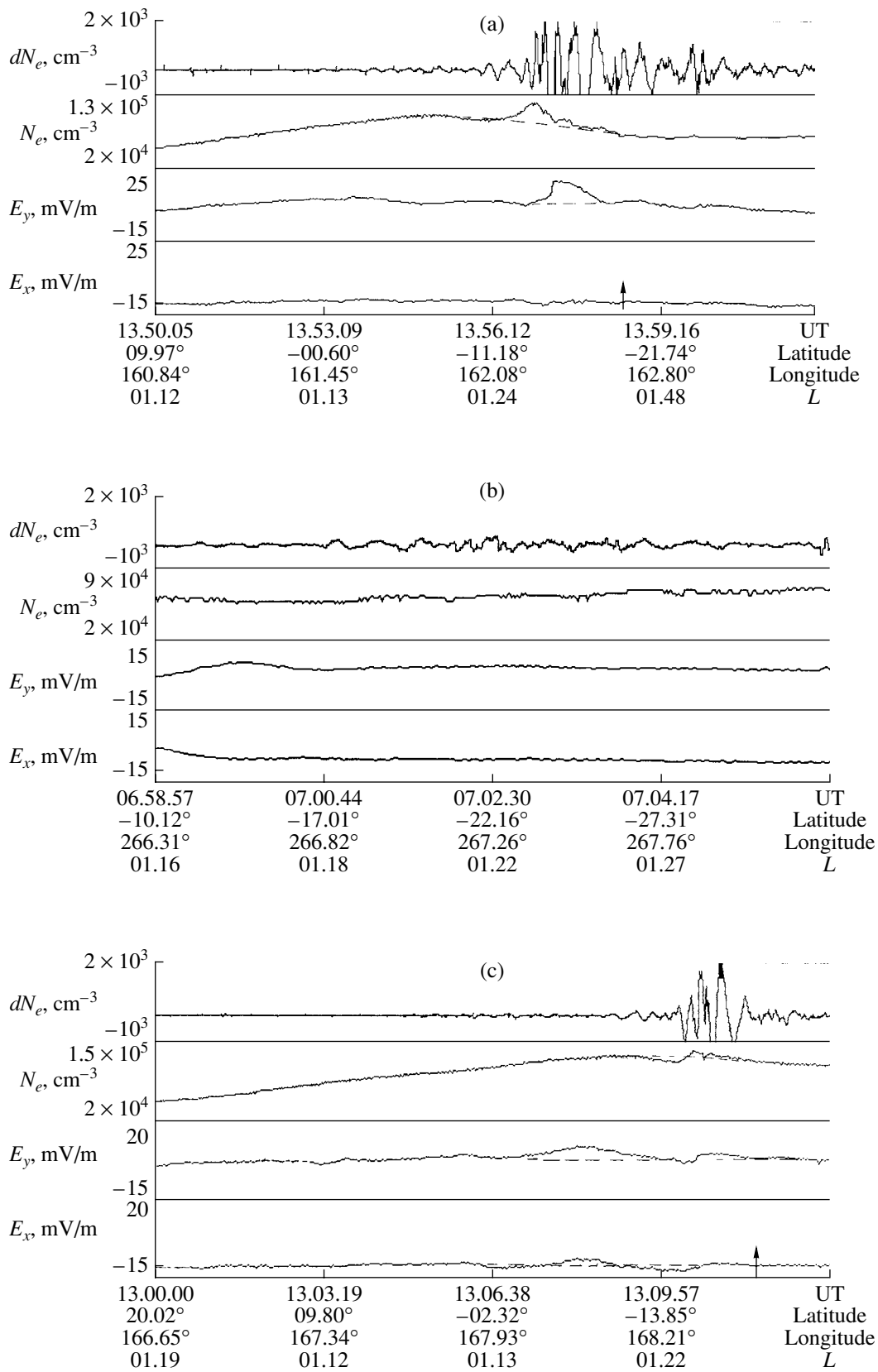


Fig. 22. Example of records of two electric field components, electron concentration, and electron concentration variations obtained on the Kosmos-1809 satellite during three flights above the HARRY typhoon region. The vertical arrow is the instant at which the satellite was closest to the typhoon center.

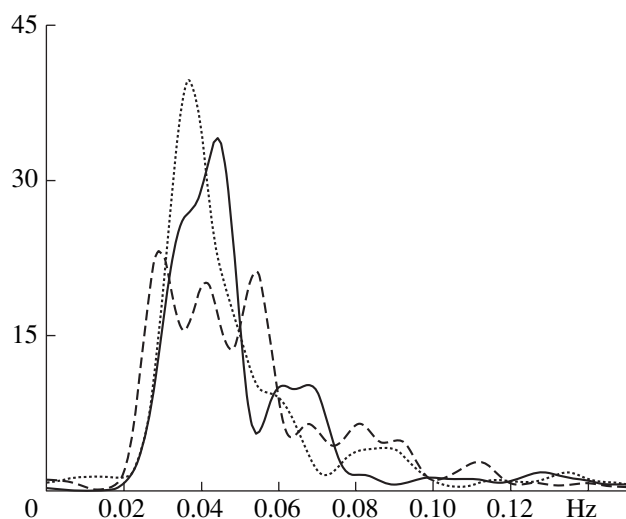


Fig. 23. Spectra of the time dependences of electron concentration perturbations obtained during three satellite flights: solid curve taken on January 27, 1989, dashed line, on February 10, 1989, and dotted line, on February 13, 1989.

10^{-7} CGSE. This would cause the appearance of a $q = 2.3$ erg/(cm² s) heat flux and an increase in the temperature of the ionosphere to 2100 K. The $N(z)$ dependences are shown in Fig. 13. Curve 1 corresponds to the unperturbed ionosphere state with an electric field of 3 mV/m, curve 2, to the ionosphere perturbed by an increase in the electric field value to 9 mV/m. It follows from these plots that an increase in the electric field increases the altitude of the F layer maximum and decreases the concentration of ions at this altitude. The character of changes in the altitude profile of the F layer is similar to that observed in probing the ionosphere from a satellite. The other recordable characteristics of the upper ionosphere state are the ionic composition and the concentration of light ions. The concentrations of hydrogen ions H⁺ measured along three orbits of the Interkosmos-24 satellite (June 20, 1990) are shown in Fig. 21. It follows from these data that the concentration of hydrogen ions reaches 6×10^3 cm⁻³ at the smallest distance from the epicenter and 2×10^3 cm⁻³ at a large distance, in the West European region. This shows that, close to an earthquake during its preparation, the concentration of ions increases approximately threefold. The results obtained using the one-dimensional model cannot be quantitatively compared with the experimental data. They however show that the mechanism of resonance recharging should cause an increase in the concentration of light ions above the region of earthquake preparation and should be taken into account in the interpretation of satellite data.

The electrodynamic model of the action of typhoon formation processes on the space plasma can serve as a basis for the search for the precursors of the catastrophic typhoon development stage and creation of a

space system for typhoon monitoring [112]. This model allows satellite electromagnetic and plasma measurement data to be related to the electrophysical and meteorological characteristics of the lower atmosphere at the typhoon formation stage. The model reduces numerous effects observed in the space plasma to a single origin, a change in the conduction current flowing in the atmosphere–ionosphere circuit. Its value and the value of the corresponding electric field are determined by the extraneous current that appears in the lower atmosphere and changes in the conductivity of the atmosphere in the typhoon formation region. At the initial typhoon formation stage (before the catastrophic phase), vapor condensation above the ocean surface occurs with the redistribution of charge carriers and changes in their mobility, which, together with vertical convection, produces the effect described above in the ionosphere–Earth electric circuit. It follows that perturbed current transfers the action of atmospheric processes responsible for the formation of typhoons into the ionosphere. The response of the ionosphere to these actions can be controlled by a measuring complex aboard a spacecraft, similar to the diagnostic complex for studying short-term earthquake precursors. Studies of electric field perturbations and electron concentration in the ionosphere above typhoon development regions were performed in [46, 47, 81, 82]. An example of data on two electric field components (E_x and E_y), electron concentration N_e , and electron concentration variations dN_e obtained by the Kosmos-1809 satellite during three flies above the HARRY typhoon on February 10 and 13, 1989 [47] are shown in Fig. 22. The vertical arrow indicates the time moment when the satellite was at a minimum distance from the typhoon center, $\sim 1.5^\circ$ east of it. Figure 22a shows that electric field and electron concentration perturbations are observed above the typhoon region. Similar results were obtained three days later in the same region (Fig. 22c). At the same time, at a large distance from the typhoon center (~ 12000 km), perturbations were absent (Fig. 22b). Electron concentration variations appear because satellites cross plasma inhomogeneities extended along the magnetic field. Spectral analysis was used to determine the spatial scale of these inhomogeneities. The spectrum calculated for the time dependences of electron concentration perturbations is shown in Fig. 23. The spectrum contains two maxima at frequencies of 0.04 and 0.07 Hz, which corresponds to periods of 25 and 14 s. At a ~ 8 km/s satellite velocity, this gives spatial inhomogeneity scales along the orbit of ~ 200 and 110 km. The spatial scales of inhomogeneities across the magnetic field are 20–40 and 10–20 km, respectively. Similar results were obtained for other typhoons; they are in agreement with the electrodynamic model described above.

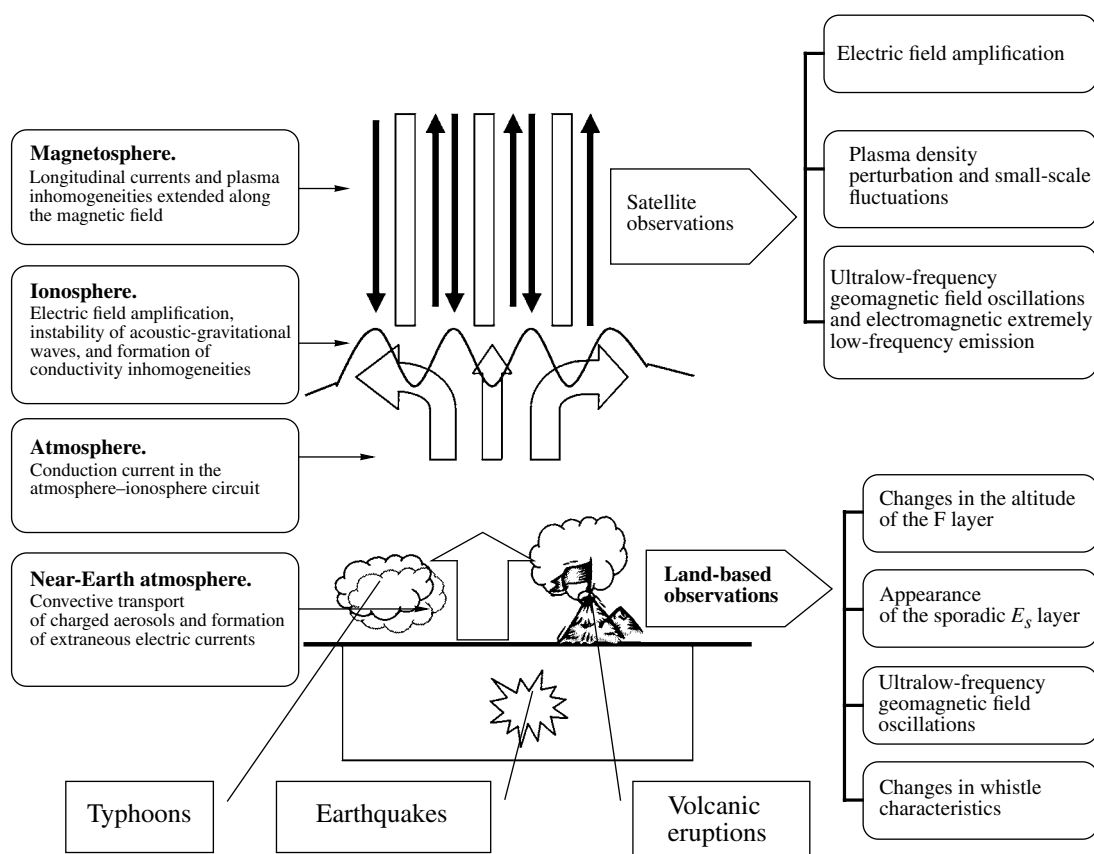


Fig. 24. Schematic representation of the electrodynamic model of the action of seismic and meteorological processes on the ionosphere.

7. CONCLUSIONS

The ionosphere, stratosphere, and troposphere make up a unified medium, the physical phenomena in which are related to each other. According to the model presented, intense processes in the lower atmosphere and lithosphere influence the plasma electrostatically in the ionosphere. Such phenomena include the preparation of earthquakes, volcanic eruptions, typhoons, lightning activity, and technogenic catastrophes. The electrophysical parameters of the lower atmosphere are related to the development of chemical, radiation, and hydrodynamic processes in it with the participation of charged aerosols. The action of seismic and meteorological phenomena on the lower atmosphere at early stages of their development causes the appearance of vertical extraneous currents and changes in the conductivity of its near-Earth layers. The electrodynamic model of the action of such phenomena on the space plasma is a combination of plasma, hydrodynamic, and electromagnetic processes that occur in the atmosphere and ionosphere. A scheme of these processes is shown in Fig. 24. It is assumed that the source of the processes constituting the model is an increase in the injection of active substances into the atmosphere and their convective transfer upward. Such substances contain charged aerosols, radioactive elements, radon in particular, their

decay products, and some gases. Their concentration increases severalfold on the eve of an earthquake or during volcanic eruption preparation. The altitude redistribution of the density of charged aerosols and an increase in the concentration of ionization sources result in the formation of extraneous currents and changes in the conductivity of the lower atmosphere. This perturbs the vertical electric current flowing between the ionosphere and Earth. An increase in the current in the ionosphere increases the electric field in it. Numerous later plasma and electromagnetic effects observed experimentally are determined by the change in the electric field in the ionospheric plasma. An increase in field in the conduction region of the lower ionosphere initiates the dissipative instability of acoustic-gravitational waves at the Brunt-Váisálá frequency. Instability results in the formation of horizontal periodic inhomogeneities of ionosphere conductivity. The interaction of these inhomogeneities with an electric field is accompanied by the generation of oblique Alfvén waves propagating upward. As a result, moving longitudinal current and plasma density layers are formed; these layers are extended along the geomagnetic field. When a satellite crosses these layers, plasma density fluctuations and ultralow-frequency magnetic field oscillations are recorded. Horizontal ionosphere

inhomogeneities are the source of extremely low-frequency radiation in magnetic field tubes because of the scattering of electromagnetic pulses from lightning discharges by them. They generate gyrotropic waves, which form geomagnetic oscillations in the ultralow-frequency range on the Earth's surface. In addition, the appearance of inhomogeneities in the nightly ionosphere results in the depression of geomagnetic pulsations of magnetospheric sources. The appearance of plasma layers causes the formation of whistle ducts in the upper ionosphere, which change the dispersion of whistles and the frequency of their appearance on the Earth's surface. Other consequences of an increase in the electric field are plasma drift, an increase in the frequency of collisions of electrons, and lower ionosphere heating because of Joule heat release. An increase in the frequency of collisions of electrons changes the amplitude and phase of superlong-wave signals during their waveguide propagation. Plasma drift and changes in the heat balance of the ionosphere are accompanied by a resonance recharging-induced increase in the concentration of light ions. The inflow of atmospheric conduction current into the ionosphere perturbs plasma density in the lower ionosphere and causes the formation of an anomalous sporadic E layer. To summarize, the model under consideration relates several observed values recorded by land-based and satellite methods to an increase in the stationary electric field in the ionosphere. This increase is caused by the intensification of ionizing factors and space charge separation processes in the lower atmosphere as seismic or meteorological activity grows.

The data obtained show that the electrodynamic model can be used as a scientific basis for the search for possible precursors of the catastrophic phase of typhoons, the creation of a method for controlling an increase in volcanic activity, and the prediction of strong volcanic eruptions dangerous for aircraft flights. The intensification of the injection of aerosols with soil gases into the atmosphere is accompanied by an increase in the temperature of near-Earth atmospheric layers. For this reason, satellite observations should include measurements of electromagnetic fields in various spectral ranges augmented by simultaneously taking photographs of the Earth's surface in the optical range.

The main conclusions are as follows:

(1) The reason for several plasma and electromagnetic phenomena observed during periods of seismic or meteorological activity increase (several days to tens of days) is electric field strengthening in the ionosphere to tens of mV/m units.

(2) Satellite data are evidence of the existence of such fields in the ionosphere, whereas, according to the land-based data, there are no visible changes in the electric field on the Earth simultaneously over distances of tens or hundreds of kilometers during earthquake preparation.

(3) Such properties are characteristic of the field of conduction current flowing in the atmosphere–ionosphere circuit. Its source is extraneous electric currents formed as a result of vertical convective transport of charged soil aerosols in the atmosphere. Aerosols get into the atmosphere from soil because of the intensification of the injection of soil gases when seismic activity increases. Field limitation is determined by the feedback relation between extraneous currents and the field on the Earth's surface. This feedback is caused by the appearance of a potential barrier to the transfer of a charged particle from soil into the atmosphere.

Because of limitations in field changes on the Earth, which can be smaller than background perturbations, satellite methods for recording fields related to seismic activity have advantages over land-based methods. In addition, field strengthening in the ionosphere can be controlled by recording plasma and electromagnetic effects caused by its response to this strengthening. The conclusion can be drawn that, because of electric field strengthening of a seismic origin, the ionosphere is a more effective field sensor than land-based measurement devices.

REFERENCES

1. M. B. Gokhberg, V. A. Morgunov, T. Yoshino, and I. Tomizawa, *J. Geophys. Res.* **87**, 7824 (1982).
2. K. Oike and T. Ogawa, *Annu. Rep., Disaster Prevention Res. Inst., Kyoto Univ.* **25**, 89 (1982).
3. V. M. Chmyrev, N. V. Isaev, S. V. Bilichenko, and G. A. Stanev, *Phys. Earth Planet. Inter.* **57**, 110 (1989).
4. O. N. Serebryakova, S. V. Bilichenko, V. M. Chmyrev, et al., *Geophys. Rev. Lett.* **19**, 91 (1992).
5. M. Parrot and F. Lefeuvre, *Ann. Geophys.* **3**, 737 (1985).
6. V. I. Larkina, V. V. Migulin, O. A. Molchanov, et al., *Phys. Earth Planet. Inter.* **57**, 100 (1989).
7. S. V. Bilichenko, A. S. Inchin, E. F. Kim, et al., *Dokl. Akad. Nauk SSSR* **311**, 1077 (1990).
8. A. C. Fraser-Smith, A. Bernardy, P. R. McGill, et al., *Geophys. Rev. Lett.* **17**, 1465 (1990).
9. O. A. Molchanov, Y. A. Kopytenko, P. M. Voronov, et al., *Geophys. Rev. Lett.* **19**, 1495 (1992).
10. M. T. Hayakawa, T. Yoshino, and V. A. Morgounov, *Phys. Earth Planet. Inter.* **77**, 97 (1993).
11. O. A. Molchanov, O. A. Mazhaeva, A. N. Golyavin, and M. Hayakawa, *Ann. Geophys.* **11**, 431 (1993).
12. Y. A. Kopytenko, T. G. Matiasvili, P. M. Voronov, et al., *Phys. Earth Planet. Inter.* **77**, 85 (1993).
13. M. Parrot, *J. Geophys. Res.* **99**, 23339 (1994).
14. V. M. Chmyrev, N. V. Isaev, O. N. Serebryakova, et al., *J. Atmos. Solar-Terr. Phys.* **59**, 967 (1997).
15. O. A. Molchanov and M. Hayakawa, *J. Geophys. Res.* **103**, 17489 (1998).
16. M. B. Gokhberg, V. A. Morgunov, and O. A. Pokhotelov, in *Seismoelectromagnetic Phenomena* (Nauka, Moscow, 1988), p. 173 [in Russian].

17. V. A. Liperovskii, O. A. Pokhotelov, and S. L. Shalimov, in *Ionospheric Earthquake Precursors* (Nauka, Moscow, 1992), p. 304 [in Russian].
18. O. A. Molchanov, in *Review of Radio Science 1990–1992*, Ed. by W. R. Stone (Oxford Univ. Press, New York, 1993), p. 591.
19. A. L. Buchachenko, V. N. Oraevskii, O. A. Pokhotelov, et al., *Usp. Fiz. Nauk* **166** (9), 1023 (1996).
20. P. Varotsos, *Acta Geophys. Pol.* **49** (1), 1 (2004).
21. *Seismo-Electromagnetics: Lithosphere–Atmosphere–Ionosphere Coupling*, Ed. by M. Hayakawa and O. A. Molchanov (TERRAPUB, Tokyo, 2002), p. 477.
22. T. R. Henderson, V. S. Sonwalkar, R. A. Helliwell, et al., *J. Geophys. Res.* **98**, 9503 (1993).
23. J. P. Matthews and J. P. Lebreton, *Ann. Geophys.* **3**, 749 (1985).
24. H. C. Koons and J. L. Roeder, in *Atmospheric and Ionospheric Electromagnetic Phenomena Associated with Earthquakes*, Ed. by M. Hayakawa (TERRAPUB, Tokyo, 1999), p. 171.
25. M. Parrot, in *Atmospheric and Ionospheric Electromagnetic Phenomena Associated with Earthquakes*, Ed. by M. Hayakawa (TERRAPUB, Tokyo, 1999), p. 685.
26. O. A. Molchanov, A. Yu. Schekotov, E. N. Fedorov, et al., *Ann. Geophys.* **47** (1), 181 (2004).
27. G. Kondo, in *Memoirs of the Kakioka Magnetic Observatory* (Kakioka, Jpn., 1968), Vol. 13, p. 17.
28. E. T. Pierce, *Geophys. Res. Lett.* **3**, 185 (1976).
29. J. Hao, *Acta Seismol. Sinica* **10**, 207 (1988).
30. J. Tate and W. Daily, *Phys. Earth Planet. Inter.* **57**, 1 (1989).
31. E. F. Vershinin, A. V. Buzevich, K. Yumoto, et al., in *Atmospheric and Ionospheric Electromagnetic Phenomena Associated with Earthquakes*, Ed. by M. Hayakawa (TERRAPUB, Tokyo, 1999), p. 513.
32. V. V. Afonin, O. A. Molchanov, T. Kodama, et al., in *Atmospheric and Ionospheric Electromagnetic Phenomena Associated with Earthquakes*, Ed. by M. Hayakawa (TERRAPUB, Tokyo, 1999), p. 597.
33. S. A. Pulinets, A. D. Legenka, and V. A. Alekseev, in *Dusty and Dirty Plasmas, Noise, and Chaos in Space and in the Laboratory* (Plenum, New York, 1994), p. 545.
34. J. Boskova, I. Smilauer, P. Triska, and K. Kudela, *Stud. Geophys. Geod.* **8**, 213 (1994).
35. V. I. Gornyi, A. G. Sal'man, A. A. Tronin, and B. V. Shilin, *Dokl. Akad. Nauk SSSR* **301**, 67 (1988).
36. A. A. Tronin, in *Atmospheric and Ionospheric Electromagnetic Phenomena Associated with Earthquakes*, Ed. by M. Hayakawa (TERRAPUB, Tokyo, 1999), p. 717.
37. Z. J. Qiang, C. G. Dian, and L. Z. Li, in *Atmospheric and Ionospheric Electromagnetic Phenomena Associated with Earthquakes*, Ed. by M. Hayakawa (TERRAPUB, Tokyo, 1999), p. 747.
38. A. A. Tronin, M. Hayakawa, and O. A. Molchanov, *J. Geodyn.* **33**, 519 (2002).
39. T. I. Toroshelidze and L. M. Fishkova, *Dokl. Akad. Nauk SSSR* **302** (2), 313 (1986).
40. G. A. Papadopoulos, in *Atmospheric and Ionospheric Electromagnetic Phenomena Associated with Earthquakes*, Ed. by M. Hayakawa (TERRAPUB, Tokyo, 1999), p. 559.
41. V. A. Alekseev and N. G. Alekseeva, *Nucl. Geophys.* **6**, 99 (1992).
42. G. I. Voitov and I. P. Dobrovolskii, *Izv. Akad. Nauk, Ser. Fiz. Zemli*, No. 3, 20 (1994).
43. H. S. Virk and B. Singh, *Geophys. Res. Lett.* **22**, 774 (1995).
44. J. Heincke, U. Koch, and G. Martinelli, *Geophys. Res. Lett.* **22**, 774 (1995).
45. G. Igarashi, T. Saeki, N. Takahata, et al., *Science* (Washington, D.C.) **269**, 60 (1995).
46. N. V. Isaev, V. M. Sorokin, V. M. Chmyrev, et al., in *Seismo-Electromagnetics: Lithosphere–Atmosphere–Ionosphere Coupling*, Ed. by M. Hayakawa and O. Molchanov (TERRAPUB, Tokyo, 2002), p. 313.
47. M. V. Sorokin, N. V. Isaev, A. K. Yashchenko, et al., *J. Atmos. Sol.-Terr. Phys.* **67**, 1269 (2005).
48. V. A. Liperovskii, C.-V. Meister, K. Schlegel, and Ch. Haldoupis, *Ann. Geophys.* **15**, 767 (1997).
49. M. B. Gokhberg, A. K. Nekrasov, and S. L. Shalimov, *Izv. Akad. Nauk, Ser. Fiz. Zemli*, No. 8, 52 (1996).
50. O. A. Molchanov, in *Atmospheric and Ionospheric Electromagnetic Phenomena Associated with Earthquakes*, Ed. by M. Hayakawa (TERRAPUB, Tokyo, 1999), p. 349.
51. V. Surkov and V. Pilipenko, in *Atmospheric and Ionospheric Electromagnetic Phenomena Associated with Earthquakes*, Ed. by M. Hayakawa (TERRAPUB, Tokyo, 1999), p. 357.
52. O. A. Molchanov, M. Hayakawa, and V. A. Rafalsky, *J. Geophys. Res.* **100**, 1691 (1995).
53. D. V. Fitterman, *J. Geophys. Res.* **84**, 6031 (1979).
54. V. A. Pilipenko, E. N. Fedorov, N. V. Yagova, and K. Yumoto, in *Atmospheric and Ionospheric Electromagnetic Phenomena Associated with Earthquakes*, Ed. by M. Hayakawa (TERRAPUB, Tokyo, 1999), p. 203.
55. L. S. Al'perovich, M. B. Gokhberg, V. M. Sorokin, and G. V. Fedorovich, *Izv. Akad. Nauk SSSR, Ser. Fiz. Zemli*, No. 3, 58 (1979).
56. V. M. Sorokin and G. V. Fedorovich, *Izv. Vyssh. Uchebn. Zaved., Radiofiz.* **25**, 495 (1982).
57. V. M. Sorokin and G. V. Fedorovich, in *Physics of Slow MHD Waves in Ionospheric Plasma* (Energoatomizdat, Moscow, 1982), p. 136.
58. O. A. Molchanov and M. Hayakawa, in *10th International Conference on Atmospheric Electricity* (Osaka, Jpn., 1996), p. 428.
59. S. A. Pulinets, V. A. Alekseev, A. D. Legen'ka, and V. V. Hegai, *Adv. Space Res.* **20**, 2137 (1997).
60. V. V. Grimalsky, M. Hayakawa, V. N. Ivchenko, et al., *J. Atmos. Sol.-Terr. Phys.* **65**, 391 (2003).
61. Y. Rapoport, V. Grimalsky, M. Hayakawa, et al., *Phys. Chem. Earth* **29**, 579 (2004).
62. Yu. G. Rapoport, *Kosmicheskaya Nauka Tekhnol.* **10** (5/6), 90 (2004).
63. J. A. Chalmers, *Atmospheric Electricity*, 2nd ed. (Pergamon, New York, 1967), p. 451.

64. V. M. Sorokin and A. K. Yashchenko, *Geomagn. Aeronomiya* **39** (2), 100 (1999) [*Geomagn. Aeronomy* **39** (2), 228 (1999)].
65. V. M. Sorokin and A. K. Yashchenko, *Khim. Fiz.* **19** (6), 71 (2000).
66. V. Sorokin and A. Yashchenko, *Adv. Space Res.* **26**, 1219 (2000).
67. V. M. Sorokin, V. M. Chmyrev, and A. K. Yashchenko, *Geomagn. Aeronomiya* **41** (2), 187 (2001) [*Geomagn. Aeronomy* **41** (2), 180 (2001)].
68. V. M. Sorokin, V. M. Chmyrev, and A. K. Yashchenko, *J. Atmos. Sol.-Terr. Phys.* **63** (16), 1681 (2001).
69. V. M. Sorokin, V. M. Chmyrev, and N. V. Isaev, *J. Atmos. Sol.-Terr. Phys.* **60**, 1331 (1998).
70. V. M. Sorokin, V. M. Chmyrev, *Geomagn. Aeronomiya* **39** (5), 38 (1999) [*Geomagn. Aeronomy* **39** (5), 574 (1999)].
71. V. M. Sorokin, V. M. Chmyrev, in *Atmospheric and Ionospheric Electromagnetic Phenomena Associated with Earthquakes*, Ed. by M. Hayakawa (TERRAPUB, Tokyo, 1999), p. 819.
72. V. M. Sorokin, V. M. Chmyrev, *Geomagn. Aeronomiya* **42** (6), 821 (2002) [*Geomagn. Aeronomy* **42** (6), 784 (2002)].
73. V. M. Sorokin, V. M. Chmyrev, and A. K. Yashchenko, *J. Atmos. Sol.-Terr. Phys.* **67**, 1259 (2005).
74. V. M. Sorokin, V. M. Chmyrev, and A. K. Yashchenko, *Adv. Space Res.* **37**, 666 (2006).
75. V. M. Sorokin, A. K. Yashchenko, V. M. Chmyrev, and M. Hayakawa, *Nat. Hazards Earth Syst. Sci.* **5**, 661 (2005).
76. N. Borisov, V. Chmyrev, and S. Rybachek, *J. Atmos. Sol.-Terr. Phys.* **63**, 3 (2001).
77. V. M. Sorokin, V. M. Chmyrev, and A. K. Yashchenko, *Geomagn. Aeronomiya* **41** (3), 327 (2001) [*Geomagn. Aeronomy* **41** (3), 315 (2001)].
78. V. M. Sorokin, V. M. Chmyrev, and A. K. Yashchenko, *J. Atmos. Sol.-Terr. Phys.* **64**, 21 (2003).
79. V. P. Kim and V. V. Hegai, in *Atmospheric and Ionospheric Electromagnetic Phenomena Associated with Earthquakes*, Ed. by M. Hayakawa (TERRAPUB, Tokyo, 1999), p. 619.
80. V. M. Sorokin and V. M. Chmyrev, in *Atmospheric and Ionospheric Electromagnetic Phenomena Associated with Earthquakes*, Ed. by M. Hayakawa (TERRAPUB, Tokyo, 1999), p. 805.
81. N. V. Isaev, V. M. Sorokin, V. M. Chmyrev, and O. N. Serebryakova, *Geomagn. Aeronomiya* **42** (5), 670 (2002) [*Geomagn. Aeronomy* **42** (5), 638 (2002)].
82. N. V. Isaev, V. M. Sorokin, V. M. Chmyrev, et al., *Kosmich. Issled.* **40** (6), 591 (2002) [*Cosmic Res.* **40** (6), 547 (2002)].
83. K. A. Boyarchuk, A. M. Lomonosov, S. A. Pulinets, and V. V. Hegai, *Stud. Geophys. Geod.* **42**, 197 (1998).
84. R. G. Fleagle and J. A. Businger, *An Introduction to Atmospheric Physics* (Academic, New York, 1963; Mir, Moscow, 1965).
85. L. D. Landau and E. M. Lifshits, *Hydrodynamics* (Nauka, Moscow, 1986), p. 736 [in Russian].
86. L. A. Gavrilova and L. S. Ivlev, *Izv. Akad. Nauk, Ser. Fiz. Atmos. Okeana* **32**, 172 (1996).
87. H. Haken, *Synergetics* (Springer, Berlin, 1978; Mir, Moscow, 1978).
88. J. H. Piddington, *Geophys. J.* **2**, 173 (1959).
89. B. N. Gershman and G. I. Grigor'ev, *Geomagn. Aeronomiya* **5** (5), 843 (1965).
90. V. M. Chmyrev, V. M. Sorokin, and O. A. Pokhotelov, in *Atmospheric and Ionospheric Electromagnetic Phenomena Associated with Earthquakes*, Ed. by M. Hayakawa (TERRAPUB, Tokyo, 1999), p. 759.
91. V. B. Lyatskii and Yu. P. Mal'tsev, *Magnetosphere-Ionosphere Interaction* (Nauka, Moscow, 1983), p. 192 [in Russian].
92. M. Hayakawa, R. Kawate, O. A. Molchanov, and K. Yumoto, *Geophys. Res. Lett.* **23**, 241 (1996).
93. V. M. Sorokin, *Geomagn. Aeronomiya* **27** (6), 925 (1987).
94. V. M. Sorokin, *Izv. Vyssh. Uchebn. Zaved., Radiofiz.* **31** (10), 1169 (1988).
95. V. M. Sorokin and A. K. Yashchenko, *Geomagn. Aeronomiya* **28**, 655 (1988).
96. V. M. Sorokin and O. A. Pokhotelov, *J. Atm. Sol.-Terr. Phys.* **67**, 921 (2005).
97. V. M. Sorokin, E. N. Fedorov, A. Yu. Schekotov, et al., *Ann. Geophys.* **47** (1), 191 (2004).
98. L. Alperovich, I. Chaikovskiy, Yu. Gurvich, and A. Melnikov, in *Seismo-Electromagnetics: Lithosphere-Atmosphere-Ionosphere Coupling*, Ed. by M. Hayakawa and O. A. Molchanov (TERRUPUB, Tokyo, 2002), p. 343.
99. H. Rishbeth and O. K. Garriott, *Introduction to Ionospheric Physics* (Gidrometeoizdat, Leningrad, 1965; Academic, New York, 1969), p. 304.
100. V. P. Kim, V. V. Hegai, and L. I. Nikiforova, *Izv. Akad. Nauk, Ser. Fiz. Zemli, No. 7*, 35 (1995).
101. S. A. Bowhill, *J. Atmos. Terr. Phys.* **24**, 503 (1962).
102. W. B. Hunson and I. B. Ortenburger, *J. Geophys. Res.* **66**, 1425 (1961).
103. T. Ondoh and M. Hayakawa, in *Seismo-Electromagnetics: Lithosphere-Atmosphere-Ionosphere Coupling*, Ed. by M. Hayakawa and O. A. Molchanov (TERRUPUB, Tokyo, 2002), p. 385.
104. T. Ondoh, *Adv. Polar Upper Atmos. Res.* **17**, 96 (2003).
105. T. Yokoyama, M. Yamamoto, R. F. Pfaff, et al., *Abstracts of Papers, 112th SGEPS Fall Meeting* (Univ. of Electro-Comm., Tokyo, 2002), p. 12.
106. V. M. Sorokin, A. K. Yashchenko, and M. Hayakawa, *J. Atmos. Sol.-Terr. Phys.* **68**, 1260 (2006).
107. H. Alfvén and C.-G. Fälthammar, *Cosmical Electrodynamics* (Clarendon, Oxford, U.K., 1963), p. 260.
108. I. M. Fuks and R. S. Shubova, *Geomagn. Aeronomiya* **34** (2), 130 (1995).
109. S. I. Martynenko, I. M. Fuks, and R. S. Shubova, *J. Atmos. Electr.* **15**, 259 (1996).
110. R. W. Schunk and A. F. Nagy, *Rev. Geophys. Space Phys.* **18**, 813 (1980).
111. V. M. Sorokin, V. M. Chmyrev, and M. Hayakawa, *Planet. Space Sci.* **48**, 175 (2000).
112. V. M. Sorokin and G. P. Cherny, *Aerospace Courier*, No. 3, 84 (1999).